

# A Global Treatment Of VMD Physics Up To The $\phi$ :

## II. $\tau$ Decay and Hadronic Contributions To $g - 2$

M. Benayoun, P. David, L. DelBuono, O. Leitner

LPNHE Paris VI/VII, IN2P3/CNRS, F-75252 Paris, France

November 3, 2021

### Abstract

Relying on the Hidden Local Symmetry (HLS) model equipped with a mechanism breaking the  $U(3)/SU(3)/SU(2)$  symmetries and generating a dynamical vector meson mixing, it has been shown that a global fit successfully describes the cross sections for the  $e^+e^- \rightarrow \pi^+\pi^-$ ,  $e^+e^- \rightarrow (\pi^0/\eta)\gamma$  and  $e^+e^- \rightarrow \pi^0\pi^+\pi^-$  annihilation channels. One extends this global fit in order to include also the dipion spectra from the  $\tau$  decay, taking into account all reported information on their statistical and systematic errors. A model accounting for lineshape distortions of the  $\rho^\pm$  spectrum relative to  $\rho^0$  is also examined when analyzing the  $\tau$  data behavior within the global fit framework. One shows that a successful account for  $e^+e^-$  annihilation data and  $\tau$  spectra can be simultaneously reached. Then, issues related with non-perturbative hadronic contributions to the muon  $g - 2$  are examined in details. It is shown that all  $e^+e^-$  data considered together allow for improved and motivated estimates for the  $a_\mu(\pi^+\pi^-)$ , the  $\pi^+\pi^-$  loop contribution to the muon  $g - 2$ ; for instance, integrated between 0.630 and 0.958 GeV, we find  $a_\mu(\pi^+\pi^-) = 359.62 \pm 1.62$  (in units of  $10^{-10}$ ), a 40% improvement of the current uncertainty. The effects of the various  $\tau$  samples in the context of a global fit procedure leads to conclude that different lineshape distortions are revealed by the ALEPH, BELLE and CLEO data samples. Relying on global fits to the data quoted above, one also provides motivated estimates of the  $\pi^+\pi^-$ ,  $\pi^0\gamma$ ,  $\eta\gamma$  and  $\pi^0\pi^+\pi^-$  contributions to  $a_\mu$  up to 1 GeV with the smallest possible uncertainties. These estimates are based on various global fit configurations, each yielding a good probability.

# 1 Introduction

It has been proved in [1] that the scope of the HLS model [2, 3], suitably broken [4], can be extended in order to include annihilation processes like  $e^+e^- \rightarrow (\pi^0/\eta)\gamma$ ,  $e^+e^- \rightarrow \pi^+\pi^-\pi^0$  and decay spectra like  $\eta/\eta' \rightarrow \pi^+\pi^-\gamma$ , beside the  $e^+e^- \rightarrow \pi^+\pi^-$  cross section. Actually, it also includes  $e^+e^- \rightarrow K^+K^-$  and  $e^+e^- \rightarrow K^0\bar{K}^0$  annihilations which have to be examined separately as they raise known specific problems [5]. Actually, most VMD physics up to the  $\phi$  meson mass is covered by our extended model [1], except for channels involving scalar mesons or channels where higher mass vector mesons could have a significant influence [6] as, seemingly,  $e^+e^- \rightarrow \omega\pi$ . However, all the  $e^+e^-$  annihilations channels examined in [1] are reasonably well described up to the  $\phi$  mass region by the model presented in [1].

The issue is now to examine how the Extended (HLS) Model performs while including other processes like the  $\tau^\pm \rightarrow \pi^\pm\pi^0\nu$  decay which is in the scope of the HLS model. This leads us to report on the results of global fits using the existing  $\tau$  dipion spectra beside the  $e^+e^-$  data extensively discussed in [1]. The same issue was partly addressed<sup>1</sup> in our former [4]. The energy range of our model is limited approximately by the  $\phi$  meson mass ; meanwhile, as far as issues like the muon  $g - 2$  value are concerned, this is an energy region where a reliable model can address some questions in a novel way.

Indeed, an interesting outcome of such a global fit is the estimate it provides for various hadronic contributions to the muon  $g - 2$ . This covers the  $\pi^+\pi^-$  loop contribution, but also those from the  $(\pi^0/\eta)\gamma$  and  $\pi^+\pi^-\pi^0$  final states. The improvements following from using simultaneously  $\tau$  data and  $e^+e^-$  data as well as the consequences of having a reliable global model describing all VMD physics up to the  $\phi$  meson mass are interesting issues. Indeed, the underlying unified (HLS) framework of our model correlates several decay channels because of their common underlying physics and phenomenological studies indicate that these physics correlations are well accepted by the data [1]. Stated otherwise, one can examine in great details several consequences of accounting for  $\tau$  decays and  $e^+e^-$  annihilations within a consistent framework.

This turns also out to readdress the long-standing problem of the discrepancy between the BNL measurement [7] of  $g - 2$  and the predictions based on  $e^+e^-$  annihilations and  $\tau$  spectra as reported in the literature [8, 9, 10, 11, 12, 13]. A quite recent study [14] tends to lessen the disagreement between these two kinds of predictions, but not to resorb it.

Our present study is based on all the  $e^+e^-$  data sets used in [1] and on the published  $\tau$  spectra. These are the dipion mass spectra collected some time ago by ALEPH [15] and CLEO [16] ; a valuable data set collected by the BELLE Collaboration, with a statistics of several million events, has been made recently available [17].

The paper is organized as follows. In Section 2, we describe the model for the dipion spectrum in the  $\tau^\pm \rightarrow \pi^\pm\pi^0\nu$  decay. The vector meson mixing produced by Isospin Breaking (IB) [1, 4] is complemented in a simple manner with another IB mechanism allowing lineshape distortions of the  $\rho^\pm$  meson mass spectrum compared with  $\rho^0$ . In this Section, we also list the  $\tau$  data sets and outline how they intervene in the global fit procedure.

In Section 3, we first emphasize the correlation between pure IB shape distortion parameters

---

<sup>1</sup>We considered together with  $e^+e^- \rightarrow \pi^+\pi^-$  cross sections, the pion form factor from ALEPH and the dipion spectrum *lineshape* from CLEO. We were, thus, less sensitive to issues related with the absolute scale of the  $\tau$  spectra.

and the absolute scale of  $\tau$  spectra. Then, the consistency of the dipion spectra from  $\tau$  decay – not affected by vector meson mixing – with all  $e^+e^-$  annihilation channels is investigated. The behavior of each  $\tau$  data set – the ALEPH [15], CLEO [16] samples and the recently issued BELLE[17] data sample – are examined under various kinds of fit conditions. It is shown that the ALEPH spectrum can be well described with simple and intuitive IB lineshape distortions compared to  $e^+e^-$ , whereas this does not work well with BELLE and CLEO spectra. The best way to account for these is rather a rescaling of the absolute scale of their spectrum. We argue that this could point towards a more complicated IB lineshape distortion model than ours. One shows, nevertheless, that a satisfactory simultaneous account of all  $e^+e^-$  annihilation data and the available dipion spectra in the  $\tau$  decay can be reached, under quite reasonable conditions.

In Section 4, we focus on the non-perturbative hadronic contributions to the muon  $g - 2$ , especially the  $\pi^+\pi^-$  one. The results provided by the various  $e^+e^- \rightarrow \pi^+\pi^-$  data sets are examined and the effects of global fits involving the  $e^+e^- \rightarrow (\pi^0/\eta)\gamma$  and  $e^+e^- \rightarrow \pi^+\pi^-\pi^0$  cross sections is shown. The effects of including the  $\tau$  dipion spectra within the fitted data sets is examined in full details. It is also shown that the KLOE data set [18] for  $e^+e^- \rightarrow \pi^+\pi^-$  does not lead to some inconsistency but, rather, allows for improved uncertainties at the expense of a worse fit probability.

We also conclude on the most likely value of several contributions to the muon  $g - 2$  following from a global fit to a large sample of  $e^+e^-$  and  $\tau$  data. The uncertainties yielded look much improved with respect to usual.

Finally, Section 5 is devoted to a summary of our conclusions. In particular, one emphasizes using the various  $\tau$  spectra in order to provide – or improve – theoretical predictions for the muon  $g - 2$ , taking into account the difficulty to model lineshape distortions in a way accepted simultaneously by the ALEPH, BELLE and CLEO data sets.

In the present paper, which is the second part of a study started in [1], one does not discuss the properties or the results of the fits to the  $e^+e^-$  data in isolation. These have been discussed at length in [1]; we also refer the reader to that paper for the details of our model. All notations have been carefully chosen in order to ensure full consistency with [1]. Finally, the present work supersedes and improves large parts of our former study [4]. We also correct here for a (minor) computer code error which affected the treatment of the sample-to-sample correlated uncertainties in the data sets from [19, 20, 21]; this is, indeed, important in order to provide reliable uncertainties to our  $g - 2$  estimates.

## 2 Including $\tau^\pm \rightarrow \pi^\pm \pi^0 \nu$ Data

The difference between  $e^+e^-$  and  $\tau$  based estimates of the hadronic contribution to the muon  $g - 2$  is an important issue. Indeed, accounting for isospin symmetry breaking effects, the  $\tau$  dipion spectra<sup>2</sup> provide predictions for the hadronic contribution which makes the expected value of  $g - 2$  close to its experimental measurement [7]. Instead, all theoretical estimates based on  $e^+e^-$  data deviate by more than  $3\sigma$ . Comprehensive discussions of this issue can be found in [8, 9, 10] and more recently in [13]. Summaries can also be found in [11, 12], for instance. A quite recent reanalysis of this discrepancy [14] concludes to a smaller disagreement between

---

<sup>2</sup>Each normalized to the world average branching ratio  $\text{Br}(\tau \rightarrow \pi\pi\nu)$ , highly influenced by the ALEPH measurement [15].

$\tau$  and  $e^+e^-$  based approaches (about  $2\sigma$ ) ; consequently, the newly proposed  $\tau$  based estimate moves farther from the BNL measurement. However, even if reduced, the mismatch between  $e^+e^-$  and  $\tau$  based estimates of the hadronic contribution to  $g - 2$  survives.

It was shown in [4] that an appropriate account of isospin symmetry breaking (IB), including its effects on the ( $\rho$ ,  $\omega$ ,  $\phi$ ) mixing, certainly solves a part of the reported discrepancy between  $e^+e^-$  and  $\tau$  spectra. However, the IB vector mixing defined there and recalled in [1] does not exhaust all effects of IB. In this paper, we examine more deeply than in [4] the effects of IB shape distortions and their connection with absolute scale issues. In order to examine this kind of IB, one needs a data sample where the  $\rho^0$  ( $e^+e^-$  annihilation) and the  $\rho^\pm$  ( $\tau$  decay) spectra are simultaneously present.

The problem of the hadronic contributions to the muon  $g - 2$  was not addressed in [4]. This issue is examined here in a wider context by revisiting the consistency pattern of the  $\tau^\pm \rightarrow \pi^\pm \pi^0 \nu$  data on one hand, and the much larger data set on the  $e^+e^- \rightarrow \pi^+\pi^-$ ,  $e^+e^- \rightarrow (\pi^0/\eta)\gamma$  and  $e^+e^- \rightarrow \pi^+\pi^-\pi^0$  annihilation channels on the other hand. This is allowed by having extended the model presented in [4] in such a way that anomalous and non-anomalous channels are implemented within the unified framework presented in [1].

Most part of the  $e^+e^- \rightarrow \pi^+\pi^-$  data sets has been commented on in [4] ; here, we only remind how the sample-to-sample correlated part of the systematic uncertainties should be treated, as this plays an important role in estimating the uncertainty on the muon  $g - 2$ . All other  $e^+e^-$  annihilation channels have been considered in details in our recent [1]. Because of the poor probability of the best fit to the KLOE data [18] already commented on in [1], the corresponding data sample is not included systematically in the set of  $e^+e^- \rightarrow \pi^+\pi^-$  data samples considered ; however, its effects will be commented upon at the appropriate places. Finally, in order to fit the parameters of our  $\rho$ ,  $\omega$ ,  $\phi$  mixing scheme [4], one still uses a subset of 9 radiative decay width data which have been taken from the latest issue of the Review of Particle Properties [22] and are given explicitly in [1].

## 2.1 The Model For $\tau^\pm \rightarrow \pi^\pm \pi^0 \nu$ Decay

Our model for the pion form factor in  $\tau$  decay coincides exactly with the formulae given in [4] :

$$F_\pi^\tau(s) = \left[ \left(1 - \frac{a}{2}\right) - \frac{ag}{2} F_\rho^\tau(s) \frac{1}{D_\rho(s)} \right] \quad (1)$$

with :

$$\begin{cases} F_\rho^\tau(s) = f_\rho^\tau - \Pi_W(s) & , \quad f_\rho^\tau = agf_\pi^2 \\ D_\rho(s) = s - m^2 - \Pi_{\rho\rho}(s) \end{cases} \quad (2)$$

where  $\Pi_W(s)$  accounts for the loop corrections to the  $\rho^\pm - W^\mp$  transition amplitude  $f_\rho^\tau$  and  $\Pi_{\rho\rho}(s)$  is the  $\rho^\pm$  self-mass. Both loops are such that they vanish at  $s = 0$ .  $g$  denotes, as usual [2, 1], the universal vector coupling and  $m^2 = ag^2 f_\pi^2$  is the  $\rho$  meson mass squared as it occurs in the HLS Lagrangian.  $a$  is the standard HLS parameter expected close to 2 [2, 4, 1].

Beside the mixing of vector mesons produced by breaking Isospin Symmetry, Reference [4] examined the possibility of having a mass difference between the neutral and charged  $\rho$  mesons. Here, we also allow for a mass squared difference between neutral and charged  $\rho$  mesons –

denoted resp.  $m^2$  and  $m^2 + \delta m^2$ . Additionally, we also allow for a coupling difference of these mesons, resp.  $g$  and  $g' = g + \delta g$ . The  $\rho^\pm - W^\mp$  transition amplitude should be modified correspondingly [4], as will be reminded shortly. These two parameters correspond within our model to allowing mass and width differences between the charged and neutral  $\rho$  mesons, as commonly done in other studies [14, 23].

### 2.1.1 The Pion Form Factor In the $\tau$ Decay

With the IB modifications just defined, the pion form factor has to be slightly modified compared with Eq. (1). It can be written :

$$F_\pi^\tau(s) = \left[ \left(1 - \frac{a}{2}\right) - F_\rho^\tau(s) g'_{\rho\pi\pi} \frac{1}{D_\rho(s)} \right] \quad (3)$$

where  $g'_{\rho\pi\pi} = ag'/2 = a[g + \delta g]/2$ . The other ingredients are modified, compared with Eqs. (1) and (2), and become :

$$\begin{cases} F_\rho^\tau(s) = f_\rho^\tau - \Pi_W(s) \\ D_\rho(s) = s - m^2 - \delta m^2 - \Pi'_{\rho\rho}(s) \\ f_\rho^\tau = f_\rho^\tau + \delta f_\rho^\tau \quad , \quad \delta f_\rho^\tau = \frac{\delta m^2}{g'} - \frac{f_\rho^\tau \delta g}{g'} \end{cases} \quad (4)$$

where  $f_\rho^\tau = agf_\pi^2$  is the  $\rho - W$  transition amplitude,  $D_\rho(s)$  is the inverse  $\rho^\pm$  propagator and  $\Pi'_{\rho\rho}(s)$  is the charged  $\rho$  self-mass. With the  $\delta f_\rho^\tau$  term in the last Eq. (4),  $F_\pi^\tau(0) = 1$  is identically fulfilled. In [4], we assumed  $\delta g = 0$ .

The (modified)  $F_\rho^\tau(s)$  is the  $W - \rho$  transition amplitude with its loop corrections. In terms of the pion  $\ell_\pi(s)$  and kaon  $\ell_K(s)$  amputated loops, one has the following expressions :

$$\begin{cases} \Pi_W(s) = g'_{\rho\pi\pi} \left[ \left(1 - \frac{a}{2}\right) \ell_\pi(s) + \frac{1}{2z_A^2} \left(z_A - \frac{a}{2}\right) \ell_K(s) \right] + P_W(s) \\ \Pi'_{\rho\rho}(s) = [g'_{\rho\pi\pi}]^2 \left[ \ell_\pi(s) + \frac{1}{2z_A^2} \ell_K(s) \right] + P_\rho(s) \end{cases} \quad (5)$$

where  $z_A = [f_K/f_\pi]^2$  is the standard SU(3) breaking parameter in the BKY breaking scheme [24, 25], while  $P_W(s)$  and  $P_\rho(s)$  are subtraction polynomials with real coefficients to be fixed by external conditions.

One could look for a motivated way, like the BKY mechanism [24], able to generate this kind of IB distortion effects. The proposed modifications look, however, reasonable and correspond to the usual way of introducing mass and width differences in other studies. This mechanism will be referred to as IB shape distortion and, if numerically relevant, may complement the IB vector mixing [4, 1].

We have checked that one can safely identify  $\ell_\pi(s)$  and  $\ell_K(s)$  – both being charged–neutral meson loops – occurring in these expressions with the amputated  $\pi^+\pi^-$  and  $K^+K^-$  loops appearing in  $e^+e^-$  annihilations [4].

In order to reduce the number of free parameters in the global fit procedure, we still identify (as in [4]) the subtraction polynomial for  $\Pi_W(s)$  with those for its partner in  $e^+e^-$  annihilation (see Section 5 in [1]). On the other hand, as one can neglect pseudoscalar meson mass differences in loop calculations, one also identifies the charged  $\rho$  self-mass  $\Pi'_{\rho\rho}(s)$  with its neutral  $\rho$  partner – up to the  $\delta g$  effect – as reminded in Section 5 of [1].

Finally, in order to fit  $\tau$  data, one has to correct for specific isospin symmetry breaking effects. For this purpose, short range [26] ( $S_{EW} = 1.0235$ ) and long range [27, 28, 29] ( $G_{EM}(s)$ ) radiative corrections have to be considered. While comparing with experimental data, the quantity in Eq. (3) has to be modified to :

$$F_\pi^\tau(s) \implies [S_{EW}G_{EM}(s)]^{1/2} F_\pi^\tau(s) \quad (6)$$

As the standard HLS model does not go beyond the lowest lying vector meson nonet, we cannot fit the whole dipion  $\tau$  decay spectrum. We chose to stop around the  $\phi$  mass [1] as, up to this energy, higher mass vector mesons seem to have a very limited influence within the channels examined in [1] and in the present work.

### 2.1.2 Useful Expressions For The Dipion Partial Width in the $\tau$ Decay

The dipion partial width in the decay of the  $\tau$  lepton can be written [4] :

$$\frac{d\Gamma_{\pi\pi}(s)}{ds} = \frac{|V_{ud}|^2 G_F^2}{64\pi^3 m_\tau^3} |F_\pi(s)|^2 G_0(s) + \mathcal{O}(\epsilon^2) \quad (7)$$

with :

$$\begin{cases} G_0(s) &= \frac{4}{3} \frac{(m_\tau^2 - s)^2 (m_\tau^2 + 2s)}{s^{3/2}} Q_\pi^3 \\ Q_\pi &= \frac{\sqrt{[s - (m_{\pi^0} + m_{\pi^+})^2][s - (m_{\pi^0} - m_{\pi^+})^2]}}{2\sqrt{s}} \end{cases} \quad (8)$$

where  $\epsilon = (m_{\pi^0}^2 - m_{\pi^+}^2)/m_{\pi^+}^2 \simeq -0.06455$ . The terms of order  $\epsilon^2$  – which manifestly break Isospin Symmetry – are negligible. On the other hand, one obviously has :

$$\frac{1}{\Gamma_{\pi\pi}} \frac{d\Gamma_{\pi\pi}(s)}{ds} = \frac{1}{N} \frac{dN(s)}{ds} \quad (9)$$

where  $\Gamma_{\pi\pi}$  is the (integrated)  $\pi\pi$  partial width in the  $\tau$  decay ;  $1/N dN(s)/ds$  is the normalized spectrum of yields over the accessible dipion invariant mass range<sup>3</sup>. While referring to  $\tau$  normalized spectra in the following, we always understand this quantity.

Using Eqs. (7) and (9) together with the customary expression [22] for the the  $\tau \rightarrow e\nu_\tau\nu_e$  partial width, one can derive :

$$|F_\pi(s)|^2 = \frac{2m_\tau^8}{|V_{ud}|^2 (m_\tau^2 - s)^2 (m_\tau^2 + 2s)} \frac{1}{\beta_-^3} \frac{\mathcal{B}_{\pi\pi}}{\mathcal{B}_e} \frac{1}{N} \frac{dN(s)}{ds} \quad (10)$$

<sup>3</sup>Of course, the total number of pion pairs is defined by  $N = \int [dN(s)/ds] ds$ .

which is the standard expression used by experimentalists to reconstruct the pion form factor from experimental data [16, 17]. In this expression  $\beta_-$  is the pion velocity in the dipion rest frame,  $\mathcal{B}_{\pi\pi}$  and  $\mathcal{B}_e$  are the branching ratios of the  $\tau$  decays to resp.  $\pi\pi\nu_\tau$  and to  $e\nu_\tau\nu_e$ .

Eq. (9) can also be written :

$$\frac{1}{\Gamma_\tau} \frac{d\Gamma_{\pi\pi}(s)}{ds} = \mathcal{B}_{\pi\pi} \frac{1}{N} \frac{dN(s)}{ds} \quad (11)$$

where  $\Gamma_\tau$  denotes the full  $\tau$  width. The theoretical expression for  $d\Gamma_{\pi\pi}/ds$  on the left-hand side is given by Eq. (7) and by  $|F_\pi(s)|^2$  as following from Subsection 2.1.1 above ; the additional factors shown by Eq. (6) are be understood. Finally, the numerical value for  $\Gamma_\tau$  – not accessible to our model – is derived from the measured lifetime [22] and  $\mathcal{B}_{\pi\pi}$  is numerically provided by each experiment with various uncertainties. Eq. (11) is the main tool in the present analysis.

### 2.1.3 Absolute Normalization of the Dipion $\tau$ Spectrum

As clear from Eqs. (6) and (7), the absolute normalization of the theoretical dipion partial width spectrum is determined by the product  $G_F^2 |V_{ud}|^2 S_{EW} G_{EM}(s)$ . Correspondingly, the absolute normalization of the experimental spectrum on the right-hand side of Eq.(11) is determined by the branching ratio  $\mathcal{B}_{\pi\pi}$ .

Less obvious analytically, but numerically important, is the role played by the universal vector coupling  $g$  and the transition amplitude  $f_\rho^{\prime\tau}$  in providing the theoretical normalization of the dipion spectrum. Indeed, as  $a$  is found numerically close to 2, Eqs. (3) and (4) show that the absolute magnitude of the dipion spectrum is proportional to the product squared of the  $\rho - W$  and  $\rho\pi\pi$  amplitudes. Therefore, actually, non-vanishing  $\delta g$  and  $\delta m^2$  influence both the lineshape and the absolute normalization of the  $\tau$  spectrum.

Moreover, one cannot exclude some other mechanism breaking CVC by modifying essentially the absolute normalization of the  $\tau$  spectra ; therefore, a correction factor  $(1 + \eta_{CVC})$  may enter Eq. (11) and can be fitted. Related with this, one should note a recent BaBar measurement about the  $\tau - \mu - e$  universality. BaBar reports<sup>4</sup> [30]  $g_\mu/g_e = 1.0036 \pm 0.0020$  as expected, while  $g_\tau/g_\mu = 0.985 \pm 0.005$  exhibits a  $3\sigma$  departure from 1. If confirmed, this may indicate a possible CVC violation in the  $\tau$  sector<sup>5</sup> affecting only the absolute scale of the  $\tau$  spectrum. On the other hand, an experimental bias on the  $\mathcal{B}_{\pi\pi}$  branching ratio cannot be excluded and could play in the same direction.

Even if very close to standard approaches, the IB lineshape distortions have been introduced here in a very simplified manner. One can easily think of a more complicated structure of these than the one we inferred.

## 2.2 Dealing With The Fitted Data Sets

Besides the data sets provided<sup>6</sup> by the ALEPH [15] and CLEO [16] Collaborations, a new sample has been recently made available by the BELLE Collaboration[17]. These are the  $\tau$  data

<sup>4</sup>We thanks W. M. Morse to have drawn our attention on this paper.

<sup>5</sup>This BaBar result contradicts a former measurement from ALEPH [15] which was consistent with lepton universality.

<sup>6</sup>As in our [4], we discard the OPAL data set [31].

sets which will be examined in conjunction with the whole set of  $e^+e^-$  data samples already considered in [1]. We remind that a subset of 9 vector meson decay partial widths is also used, corresponding to decay modes not related with the annihilation data considered in our fit procedure ; these are numerically extracted from [22].

### 2.2.1 The $\tau$ Input To The Fit Procedure

In the present study, we submit to fit the experimental spectra as shown in the right-hand side of Eq. (11). In order to remain consistent, we use for each experiment its own published branching ratio measurement and not the world average branching ratio.

As for the CLEO data, our input is their published spectrum [16] for  $1/NdN(s)/ds$  normalized to their latest updated branching ratio measurement[32, 22],  $\mathcal{B}_{\pi\pi} = (25.36 \pm 0.44)\%$ . This Collaboration also claims an uncertainty on the absolute energy scale [16, 33] of about 0.9 MeV. However, in our former analysis [4], no such uncertainty showed up significantly. Anticipating somewhat on our present analysis, we confirm its effective consistency with zero and, therefore, discard this freedom from now on.

Concerning the ALEPH data, we use directly the last update of the  $\mathcal{B}_{\pi\pi}/NdN(s)/ds$  spectrum [15]. The corresponding branching fraction,  $\mathcal{B}_{\pi\pi} = (25.471 \pm 0.097 \pm 0.085)\%$ , is the most precise among the published measurements. The uncertainties will be added in quadrature (0.127%).

For the BELLE data [17], we have been provided [34] with all information concerning the pion form factor spectrum<sup>7</sup>, its covariance matrix for statistical errors and its systematics. The systematics have been added in quadrature to the statistical error covariance matrix. The BELLE  $1/NdN(s)/ds$  spectrum data are published as such [17] ; its error covariance matrix can be derived from the corresponding information provided for the pion form factor, using simple algebra. As stated above, we have submitted to fit the BELLE  $\mathcal{B}_{\pi\pi}/NdN(s)/ds$  spectrum normalized to the BELLE branching ratio [17]  $\mathcal{B}_{\pi\pi} = (25.34 \pm 0.39)\%$ .

The uncertainty provided by the branching ratio error is clearly a scale uncertainty and a bin-to-bin correlated error ; this should be treated as reminded in Section 6 of [1]. This turns out to define the (partial)  $\chi^2$  for each of the ALEPH, BELLE and CLEO data sets by [1] :

$$\chi_{Exp}^2 = [(1 + \lambda_{Exp})m_i - f(s_i)][(1 + \lambda_{Exp})m_j - f(s_j)]V_{ij}^{-1} + \left[ \frac{\lambda_{Exp}}{\eta_{Exp}} \right]^2 \quad (12)$$

having defined, for each experiment, the measurements  $m_i$  as the central value for the branching ratio times  $1/NdN(s_i)/ds$  and  $V$  being the full error covariance matrix.  $f(s_i)$  should be understood as the left-hand side of Eq. (11) computed at the appropriate energy point.

For each experiment,  $\lambda$  is a scale parameter to be fitted and  $\eta$  is the ratio of the branching ratio uncertainty to its central value. The second term in this  $\chi^2$  is the standard way to account for a scale uncertainty. We have  $\eta_{CLEO} = 1.74\%$ ,  $\eta_{ALEPH} = 0.51\%$  and  $\eta_{BELLE} = 1.53\%$ .

With this input to the fit procedure, the ALEPH, BELLE and CLEO data sets are clearly treated on the same footing. As emphasized in [1], if for some experiment the ratio  $\lambda_{fit}/\eta_{Exp}$  is small enough (typically not greater than  $\simeq 1 \div 2$ ), one can neglect this scale correction and

---

<sup>7</sup> Normalized to the world average branching ratio  $\text{Br}(\tau \rightarrow \pi^+\pi^-\nu)$ , four times more precise than the BELLE own measurement, and slightly shifted.



use the standard  $\chi^2$  expression in the minimization procedure, with the replacement  $V_{ij} \Rightarrow V_{ij} + \eta_{Exp}^2 m_i m_j$ . Otherwise, one may consider we are faced with some missing variance and keep Eq. (12) as it stands.

In a previous study [4], we limited ourselves to considering only the  $\tau$  data points up to 0.9 GeV in order to avoid at most effects of higher mass vector mesons. In the present work, however, preliminary studies using the BELLE and CLEO data<sup>8</sup> samples lead us to push this upper energy limit up to 1.0 GeV. Indeed, as in our  $e^+e^-$  fit studies [1], the influence of higher mass vector mesons seems negligible all along the energy region from threshold to 1.0 GeV – and even slightly above ; therefore, there is no physical ground to abstain from such an extension of the fitting range.

### 2.2.2 Testing The $\tau$ Spectrum Lineshapes

The remarks presented in Subsection 2.1.3 explain why it is certainly appropriate to test the various  $\tau$  spectrum lineshapes independently from their absolute magnitudes. This can be done in two different ways.

A first method turns out to normalize the data points  $m_i$  to the sum of the data points covered by our fitted energy range (from threshold up to 1 GeV/c). Then, correspondingly, the model function  $f(s)$  on the left-hand side of Eq. (11) should be normalized to its integral over the fitted range.

Another method, is simply to minimize the  $\chi^2$  as defined by Eq. (12), but amputated this from the  $(\lambda/\eta)^2$  term which constrains the scale in accordance with the claimed experimental uncertainty. Indeed, in this way, the scale factor is allowed to vary freely within the global fit procedure. We checked that these two methods give similar results.

### 2.2.3 Dealing With The Uncertainties In $e^+e^-$ Data Samples

Uncertainties in the  $e^+e^-$  data sets are accounted for in several ways. For the  $e^+e^- \rightarrow \pi^0\gamma$  data sets [35, 36, 37] and the  $e^+e^- \rightarrow \eta\gamma$  data sets [38, 39, 35, 36, 40], taking into account the magnitude of the systematics, we did not find motivated to split them up into their bin-to-bin correlated and uncorrelated parts. We just add in quadrature the reported systematic and statistical errors.

For the  $e^+e^- \rightarrow \pi^+\pi^-\pi^0$  samples, we dealt differently with the different data sets. For the relatively unprecise data sets [41, 42] we did as just explained for  $e^+e^- \rightarrow (\pi^0/\eta)\gamma$  data and simply added systematic and statistical errors in quadrature. Instead, for the more accurate data sets [19, 43, 44, 45], only the uncorrelated part of the systematic uncertainty has been added in quadrature to the statistical errors. On the other hand, the bin-to-bin correlated error has been treated as emphasized above for the  $\tau$  data sets. For reasons already emphasized in [1], we have discarded the  $e^+e^- \rightarrow \pi^+\pi^-\pi^0$  data provided by [46, 47].

Finally, the various Novosibirsk  $e^+e^- \rightarrow \pi^+\pi^-$  data sets recently collected [19, 20, 48, 21] carry a common bin-to-bin *and* sample-to-sample correlated uncertainty of 0.4 %. The older data from OLYA and CMD [49] also share a common correlated (scale) uncertainty [50] of

---

<sup>8</sup>For instance, fitting the BELLE and CLEO spectrum lineshapes up to 1. GeV does not reveal worse fit quality than when stopping the fit at 0.9 GeV. Higher mass vector meson influence in this region, if any, is thus found small enough to be absorbed by the other fit parameters.

$\simeq 1\%$ . In both cases, we have added the uncorrelated part of the systematics to the statistical errors in quadrature.

Instead, in order to treat properly the correlated uncertainty, one should consider the data sets in [19, 20, 48, 21] as a single (merged) data set and use as  $\chi^2$  an expression like Eq. (12) to introduce the common scale to be fitted. Here also, if  $\lambda/0.4\% \leq 1 \div 2$ , one could remove this scale while performing the change  $V_{ij} \Rightarrow V_{ij} + (0.4\%)^2 m_i m_j$ . One has performed the same way, *mutatis mutandis*, with the older OLYA and CMD data sets [49].

Because of the poor probability of the best fit to the KLOE data [18] already commented upon in [1], the corresponding data sample is not included systematically in the set of  $e^+e^- \rightarrow \pi^+\pi^-$  data samples considered ; however, its effects will be noted when relevant. In order to fit the parameters of the IB  $\rho$ ,  $\omega$ ,  $\phi$  mixing scheme [4, 1], one still uses a subset of 9 radiative decay width data which are taken from the latest issue of the Review of Particle Properties [22] and are given explicitly in [1].

### 3 Simultaneous Fits To $e^+e^-$ and $\tau$ Data

#### 3.1 Interplay Between $\delta m^2$ , $\delta g$ And $\lambda$

Strictly speaking, the lineshape of the  $\tau$  spectrum is determined by the HLS parameters  $g' = g + \delta g$  and the Higgs–Kibble mass  $m^2 + \delta m^2$ . This is clear from the expressions given in Section 2 above. The specific Isospin breaking parameters  $\delta m^2$  and  $\delta g$  differentiate the  $\rho^\pm$  lineshape from those of the  $\rho^0$  meson. However, these parameters also govern the absolute scale of the  $\rho^\pm$  spectrum compared to the  $\rho^0$  one. Therefore, if an uncertainty on the absolute scale of a measured  $\tau$  spectrum calls for a fit parameter  $\lambda$  rescaling the whole data spectrum, it is quite important to examine its interplay with  $\delta g$  and  $\delta m^2$ .

Data Set	$\delta m^2$ (GeV <sup>2</sup> )	$\delta g$	$\lambda$	$[\chi^2/points]_{Exp}$
ALEPH	$(3.37 \pm 1.27) 10^{-3}$	$(-0.56 \pm 0.12) 10^{-1}$	$(-1.01 \pm 0.40)\%$	27.16/38
BELLE	$(-0.01 \pm 0.77) 10^{-3}$	$(-0.12 \pm 0.10) 10^{-1}$	$(-3.83 \pm 0.54)\%$	32.46/20
CLEO	$(-1.53 \pm 1.07) 10^{-3}$	$(0.16 \pm 0.14) 10^{-1}$	$(-5.51 \pm 0.74)\%$	38.99/30
ALEPH	$(4.04 \pm 1.22) 10^{-3}$	$(-0.69 \pm 0.11) 10^{-1}$	<b>0</b>	29.19/37
BELLE	$(2.18 \pm 0.71) 10^{-3}$	$(-0.51 \pm 0.08) 10^{-1}$	<b>0</b>	41.12/19
CLEO	$(2.26 \pm 0.94) 10^{-3}$	$(-0.54 \pm 0.11) 10^{-1}$	<b>0</b>	61.49/29

Table 1: Global fit results with each  $\tau$  data sample separately. Boldface numbers are actually not allowed to vary in the fits. Global fit probabilities are always above 90%.

For the present exercise, we consider all data sets involving  $e^+e^- \rightarrow \pi^+\pi^-$  data together with all data sets covering the  $e^+e^- \rightarrow \pi^0\gamma$  and  $\eta\gamma$  annihilation channels. These additional channels allow to remove the  $\rho^0/\omega/\phi \rightarrow (\pi^0/\eta)\gamma$  partial widths from the vector meson decay

mode subsample unavoidably used. In this Section, the ISR KLOE data sample for  $e^+e^- \rightarrow \pi^+\pi^-$  is removed from the collection of data sets to be fitted ; we also leave aside the  $e^+e^- \rightarrow \pi^+\pi^-\pi^0$  annihilation data which play a minor role in defining the vector meson mixing scheme.

The  $e^+e^-$  measurements with  $s < 1.05 \text{ GeV}^2$  are submitted to fit – in order to include the  $\phi$  region – together with all  $\tau$  decay measurements with  $m_{\pi\pi} < 1 \text{ GeV}$ .

We have performed simultaneous fits of each of the A, B and C  $\tau$  data sets together with the  $e^+e^-$  data referred to above. The results are shown in Table 1 and exhibit quite interesting features, depending on the particular  $\tau$  data set considered.

The first three lines provide parameter values when  $\delta m^2$ ,  $\delta g$  and  $\lambda$  are allowed to vary. For each  $\tau$  data sample,  $\lambda$  is constrained by the relevant  $[\lambda_{fit}/\eta_{Exp}]^2$  term in the global  $\chi^2$ . In this case, one notes that :

- The significance for a non-zero  $\delta m^2$  is at  $\simeq 2.6 \sigma$  for A and negligible for B or C ,
- The significance for a non-zero  $\delta g$  is at the  $\simeq 1 \sigma$  level for B or C but large for A ( $4.7\sigma$ ),
- The values for some important correlation coefficients returned by the fit are large for each  $\tau$  data set :  $(\delta g, \lambda) \simeq (\delta g, \delta m^2) \simeq -50 \%$  and  $(\lambda, \delta m^2) \simeq (25 \div 50) \%$ . These values reflect the interplay between  $\delta g$ ,  $\delta m^2$  and  $\lambda$  in determining the absolute scales of the experimental spectra.
- The significance for non-zero  $\lambda$ 's is data set dependent :  $2.5 \sigma_\lambda$  for A,  $7.1\sigma_\lambda$  for B and  $7.40\sigma_\lambda$  for C. Compared with the scale uncertainties induced by the errors on the respective  $\mathcal{B}_{\pi\pi}$ , this corresponds to  $[\lambda_{fit}/\eta]_{ALEPH} = 2.0 \pm 0.8$ ,  $[\lambda_{fit}/\eta]_{BELLE} = 2.5 \pm 0.35$  and  $[\lambda_{fit}/\eta]_{CLEO} = 3.2 \pm 0.43$ . Taking into account the large correlations, between  $\delta g$ ,  $\delta m^2$  and  $\lambda$ , this looks to us acceptable.

The corresponding fit residuals are shown superimposed in the upmost Figure 1. One clearly sees that the B and C residuals are well spread around zero. Those for A are slightly distorted around the  $\rho$  peak in a way opposite to B and C. The last data column in Table 1 illustrates that each of A, B and C is well described by the global fit, simultaneously with  $e^+e^-$  data (The so-called New Timelike data [19, 20, 21] always yield  $\chi^2/points \simeq 118/127$ ).

The non-zero values for the  $\lambda$ 's could possibly mean that the reported measured values for  $\mathcal{B}_{\pi\pi}$  are overestimated. However, the large correlations noted just above prevent such strong a conclusion, as the rescaling effect could well be absorbed by some different values for  $(\delta g, \delta m^2)$ .

It is, therefore, worth examining the case when  $\lambda \equiv 0$  is imposed. Of course, this turns out to prevent any rescaling of the experimental spectra and, thus, check whether the mass and coupling breaking we introduced could account alone for the measured reported normalizations of the various  $\tau$  spectra. The corresponding results are shown in the downmost three lines of Table 1 and call for important remarks :

- The significance for a non-zero mass shift  $\delta m^2$  is always improved :  $3.6 \sigma$  for A,  $3.1 \sigma$  for B and  $2.4 \sigma$  for C,

- The coupling difference always becomes highly significant : the ratio of the central value to its uncertainty is 6.3 for A and B and 4.9 for CLEO.
- However, fixing  $\lambda \equiv 0$  marginally degrades the BELLE description, more significantly the account of CLEO data, whereas the fit quality is unchanged – and quite good – for ALEPH data.

The description of  $e^+e^-$  data are, in this case, marginally degraded (The new timelike data, for instance yield  $\chi^2 \simeq 125$  instead of 118 before).

This leads us to conclude that the additional Isospin Symmetry breaking mechanism, which summarizes into mass and width differences for the  $\rho$ 's, allows to account for the original absolute normalization of the ALEPH spectrum with a very good probability. One can thus conclude that the dipion ALEPH spectrum – or, equivalently, the ALEPH pion form factor – is in full accord with VMD predictions, *provided one suitably accounts for mass and width shifts in the  $\rho^\pm$  information compared to  $\rho^0$* . Numerically, this turns out to plug into the ALEPH spectrum parametrization :

$$\begin{cases} \frac{\Gamma_{\rho^\pm} - \Gamma_{\rho^0}}{\Gamma_{\rho^0}} \simeq \frac{2\delta g}{g} = [-2.50 \pm 0.40] \% \\ m_{\rho^\pm}^2 - m_{\rho^0}^2 = \delta m^2 = (4.04 \pm 1.22) 10^{-3} \text{ GeV}^2 \end{cases} \quad (13)$$

which approximately<sup>9</sup> means  $m_{\rho^\pm} - m_{\rho^0} \simeq 2.59 \pm 0.78$  MeV and  $\Gamma_{\rho^\pm} - \Gamma_{\rho^0} \simeq -3.7 \pm 0.6$  MeV. If  $\delta m^2$ , is numerically in the usual ballpark [22],  $\delta g$  seems slightly larger than could have been inferred from commonly reported estimates [22, 23] for  $\Gamma_{\rho^\pm} - \Gamma_{\rho^0}$ .

The results corresponding to fits with  $\lambda = 0$  are shown in the downmost Figure 1. Compared with the upmost one, this Figure shows interesting features : the ALEPH residual distribution is essentially unchanged, but the residuals for BELLE and CLEO are shifted towards positive values and start resembling the ALEPH residual distribution. This indicates graphically that some rescaling is still needed in order to get a satisfactory description of the B and C data sets. Whether this residual rescaling could be absorbed into a more sophisticated Isospin breaking distortion mechanism cannot be discarded.

As a summary, one can assert that, with appropriately chosen  $\delta m^2$  and  $\delta g$ , ALEPH data can avoid any significant rescaling within the model we developed. This attractive property is unfortunately not completely shared by BELLE and CLEO in isolation. This is reflected by the fit information given in the last data column of Table 1 and by the downmost Figure 1. Nevertheless, with some rescaling, the BELLE and CLEO data sets can be satisfactorily understood.

Moreover, it is clear from the above analysis that there is a large interplay between parameters defining IB shape distortions and the absolute scale of the experimental spectra. Stated otherwise, some part of a fitted rescaling could be due to the difficulty to model the actual shape distortions and, conversely, some part of a real scale factor could well be absorbed by a fitted distortion. Therefore, one cannot claim, in view of a large fitted rescaling, that the reported  $\mathcal{B}_{\pi\pi}$  should be rescaled by as much.

---

<sup>9</sup>Mass and width of broad objects like the  $\rho$  are, conceptually, definition dependent and, additionally, we have not accounted for the large negative correlation term ( $\delta g, \delta m^2$ ). Moreover, these numerical values somewhat vary, depending on the exact  $e^+e^-$  data set content submitted to the global fit.

## 3.2 Fitting The $\tau$ Lineshapes

In view of the different behaviors of the A, B and C data sets, it is worth examining separately the  $\tau$  spectrum lineshapes besides the full spectra. As explained in Subsection 2.2.2, this turns out to fit the  $\tau$  data samples without including the scale constraining terms in their contributions to the total  $\chi^2$ .

For this purpose, one has first performed a global fit leaving free  $\delta m^2$ ,  $\delta g$  and the  $\lambda$ 's unconstrained. One thus gets  $\delta g = (0.15 \pm 0.08) 10^{-1}$  and  $\delta m^2 = (-1.47 \pm 0.67) 10^{-3} \text{ GeV}^2$  with<sup>10</sup>  $\chi_{ALEPH}^2 = 17.86$ ,  $\chi_{BELLE}^2 = 29.37$  and  $\chi_{CLEO}^2 = 29.71$  associated with a  $\chi^2 = 118.31$  for the 127 data points of the so-called New Timelike data [19, 20, 48, 21]. Instead, when imposing  $\delta g = \delta m^2 = 0$ , one gets  $\chi_{ALEPH}^2 = 19.22$ ,  $\chi_{BELLE}^2 = 27.61$  and  $\chi_{CLEO}^2 = 31.83$  while the New Timelike data get  $\chi^2 = 120.23$ .

One may compare the  $\chi^2$  values yielded for each of the  $\tau$  data samples when fitting together their normalized spectra with those already reported<sup>11</sup> in Table 1.

The results given just above enforce the conclusions we reached in Subsection 3.1. In the global fit procedure, it looks difficult to distinguish effects due to IB shape distortions in the  $\rho$  distribution from genuine rescaling effects. This is especially striking when considering the ALEPH data set : One gets a quite acceptable description of the invariant mass distribution by either assuming  $\lambda = 0$  and  $(\delta g, \delta m^2)$  free or by letting  $\lambda$  free and imposing  $\delta g = \delta m^2 = 0$ . So, the reported scale discrepancy can be absorbed ; however, the sharing of the effect between true (physical) lineshape distortions and an (experimental) bias in the accepted value for  $\mathcal{B}_{\pi\pi}$  is beyond the scope of fit results. This is an important issue for using  $\tau$  data in order to estimate hadronic contributions to  $g - 2$  ; this will be commented on at the appropriate place.

Therefore, at least when fitting the  $\tau$  lineshapes, it is not justified to keep non-vanishing  $\delta m^2$  and  $\delta g$ . In this case, the main difference between the  $\rho^+$  and the (physical)  $\rho^0$  is essentially carried [4, 1] by the  $\gamma - \rho^0$  and the  $W - \rho^\pm$  transition amplitudes  $f_\rho^\gamma$  and  $f_\rho^\tau$  :

$$\frac{f_\rho^\gamma}{f_\rho^\tau} = 1 + \frac{1}{3}\alpha(s) + \frac{z_V\sqrt{2}}{3}\beta(s) \quad , \quad (f_\rho^\tau = ag^2f_\pi^2) \quad (14)$$

These amplitudes differ through terms explicitly depending on the Isospin Symmetry breaking functions which account for the vector meson mixing [4, 1]. The  $s$ -dependent terms in Eq. (14) account for the isospin zero component of the  $\rho^0$  meson. Keeping non-vanishing  $\delta g$  and  $\delta m^2$  within our modelling, the right-hand side of Eq. (14) gets a leading additional  $(\delta m^2/m^2 - \delta g/g)$  term.

From now on, we choose to reintroduce the  $e^+e^- \rightarrow \pi^+\pi^-\pi^0$  data from [41, 42] and [19, 43, 44, 45], as discussed in Subsection 2.2.3 above. We also let the scale factors vary for both the  $e^+e^-$  and  $\tau$  data sets<sup>12</sup>. Some numerical results obtained with various data set configurations are reported in Table 2. One notes that all scale factors introduced for the  $e^+e^- \rightarrow \pi^+\pi^-$  and  $e^+e^- \rightarrow \pi^0\pi^+\pi^-$  cross sections are in good correspondence with the

<sup>10</sup>The number of data points in the  $\tau$  data samples submitted to fit are always 37 (A), 19 (B) and 29 (C).

<sup>11</sup>Let us remind that the fit results reported in this Table are, instead, obtained from (global) fits using each of the  $\tau$  data sets in isolation.

<sup>12</sup>keeping, of course, the term constraining the scale variation for all the relevant data sets.

	Expected	No $\tau$ Data		$\tau$ Data Set Configurations	
	r.m.s.	$e^+e^-$ NSK+KLOE	$e^+e^-$ NSK	NSK + $A^{sh}B^{sh}C^{sh}$	NSK + ABC
Scale New Timelike	0.4%	$(-0.9 \pm 0.4)\%$	$(-0.6 \pm 0.4)\%$	$(-0.6 \pm 0.4)\%$	$(+0.4 \pm 0.3)\%$
Scale Old Timelike	1.0%	$(+1.4 \pm 0.7)\%$	$(+1.6 \pm 0.7)\%$	$(+1.6 \pm 0.7)\%$	$(+2.4 \pm 0.7)\%$
Scale CMD-2 [19]	1.3%	$(-0.4 \pm 1.2)\%$	$(-0.5 \pm 1.2)\%$	$(-0.4 \pm 1.2)\%$	$(-0.7 \pm 1.2)\%$
Scale CMD-2 [43]	2.5%	$(-2.6 \pm 1.9)\%$	$(-1.8 \pm 1.9)\%$	$(-1.8 \pm 1.9)\%$	$(-1.4 \pm 1.9)\%$
Scale CMD-2 [44]	4.6%	$(-4.7 \pm 3.4)\%$	$(-4.2 \pm 3.4)\%$	$(-4.1 \pm 3.5)\%$	$(-3.6 \pm 3.4)\%$
Scale CMD-2 [45]	1.9%	$(-2.6 \pm 1.6)\%$	$(-2.2 \pm 1.6)\%$	$(-2.0 \pm 1.6)\%$	$(-2.1 \pm 1.6)\%$
$g$	—	$5.569 \pm 0.003$	$5.587 \pm 0.008$	$5.565 \pm 0.006$	$5.532 \pm 0.007$
$\delta g$	—	—	—	<b>0</b>	$[-0.30 \pm 0.07] 10^{-1}$
$\delta m^2$ (GeV <sup>2</sup> )	—	—	—	<b>0</b>	$[1.09 \pm 0.6] 10^{-3}$
$x$	—	$0.917 \pm 0.012$	$0.908 \pm 0.013$	$0.905 \pm 0.013$	$0.902 \pm 0.013$
$z_A$	—	$1.501 \pm 0.010$	$1.476 \pm 0.009$	$1.468 \pm 0.009$	$1.454 \pm 0.009$
$a$	—	$2.372 \pm 0.002$	$2.357 \pm 0.005$	$2.361 \pm 0.004$	$2.382 \pm 0.004$
$c_3$	—	$0.927 \pm 0.006$	$0.936 \pm 0.006$	$0.944 \pm 0.006$	$0.952 \pm 0.006$
$c_1 - c_2$	—	$1.194 \pm 0.031$	$1.196 \pm 0.032$	$1.228 \pm 0.032$	$1.237 \pm 0.032$
$\chi^2/\text{dof}$	—	647.43/653	521.15/593	602.36/675	645.22/676
Probability	—	55.4%	98.5%	97.9%	79.7%

Table 2: Results in various fit configurations.  $e^+e^-$  NSK data stand for all annihilation processes discussed in the text. Inclusion of ALEPH, BELLE and CLEO data are referred to as A, B and C spectra respectively,  $A^{sh}$ ,  $B^{sh}$  and  $C^{sh}$  denote the corresponding normalized spectra. The upper part displays the rescaling factors for  $\pi^+\pi^-$  (first two lines) and  $\pi^+\pi^-\pi^0$  data samples. The lower part refers to breaking parameters discussed in Ref. [1]. Numbers written boldface are parameter values not allowed to vary inside fits.

expectations reminded in the first data column. This result is understood as confirming once more [1] the claims of the corresponding experiments concerning their correlated systematic uncertainties. In the same Table, the data column  $A^{sh}B^{sh}C^{sh}$  reports the results obtained while removing the scale constraining terms (the second one in Eq. (12) for each  $\tau$  data sample). The

numerical values of the rescaling parameters for the  $\tau$  spectra are given below.

Table 2 justifies the removal of the  $e^+e^-$  rescaling factors<sup>13</sup> from the set of parameters to be fitted. One also observes that the physics parameters have only (small) reasonable fluctuations. Finally, Table 2 clearly shows that all Novosibirsk (NSK) data (4 different cross sections) are quite consistent with the freely rescaled  $\tau$  decay data as the fit yields a probability above the 90% level. Moreover, it is also interesting to note that constraining the rescaling of the  $\tau$  spectra by their reported scale uncertainty (*i.e.*, keeping the scale fixing terms as in Eq. (12)) still provides quite comfortable probabilities (above the 80% level), as can be seen from the last data column in Table 2.

This last data column exhibits also interesting features : In a simultaneous fit to all  $\tau$  data samples together with  $e^+e^-$  data and vector meson decay modes, the significance for a non-vanishing  $\delta g$  is  $\simeq 4\sigma$  whereas that for  $\delta m^2$  is only  $\simeq 1.8\sigma$ . Comparing with the separate  $\tau$  data sample fits reported in Table 1 indicates that significantly non-vanishing  $\delta m^2$  and  $\delta g$  are driven by ALEPH data only.

We have explored the effect of including the KLOE data set [18] beside the whole set of Novosibirsk  $e^+e^-$  data and the three  $\tau$  decay data sets. As expected from its intrinsically large  $\chi^2$  [1] (123 for 60 measurements in the present case), the global fit probability drops to  $\simeq 8\%$ . However, the information displayed in Table 2 is not substantially modified. In particular, the scale factors affecting the  $e^+e^-$  Novosibirsk data remain very close to the expectations reported in the first data column.

From now on, all scale factors affecting the  $e^+e^-$  data – except for KLOE, when relevant – are set to zero and the scale uncertainties are transferred into the error covariance matrix as explained above and emphasized in Section 6 of [1].

### 3.3 Final Global Fits To $e^+e^-$ and $\tau$ Data

In this Subsection, we only refer to fits performed without the KLOE data set. Some results are displayed in Table 3 and will be discussed now ; other pieces of information will be given later on, especially those with each  $\tau$  data sample fitted in isolation with the whole set of  $e^+e^-$  data.

Two kind of results are shown in Table 3, the former with fitting only the  $\tau$  spectrum lineshapes<sup>14</sup> (see Subsection 2.2.2 above), the later with the full  $\tau$  spectrum information as expressed by Eq. (11). The first data column in Table 3 displays the results obtained with only the whole set of  $e^+e^-$  data [1].

The first two data columns in Table 3 clearly illustrate that the fit quality remains optimum<sup>15</sup> (above the 90% level) when including only the  $\tau$  spectrum *lineshapes* inside the fit procedure (data column flagged with  $A^{sh}$   $B^{sh}$   $C^{sh}$ ). This does not hide some badly described data set as reflected by the various partial  $\chi^2$  displayed. Figure (2) displays the normalized spectra together with the fit function ; the residual distributions shown in Figure (3) confirm the goodness of the fit.

<sup>13</sup>Then, the correlated scale uncertainties only appear in the full error covariance matrix as reminded in Subsection 2.2.3 and in Section 6 of [1].

<sup>14</sup>In this case, the  $\tau$  data are flagged as  $A^{sh}$ ,  $B^{sh}$  and  $C^{sh}$  for respectively the ALEPH, BELLE and CLEO data sets. When using, for each  $\tau$  data set, the full Eq. (12), these data sets are simply flagged A, B and C.

<sup>15</sup>The origin of such favorable probabilities is discussed at the end of this Subsection.

Comparing the individual  $\chi^2$  in the second data column with those in the first one for the different  $e^+e^-$  data subsets (and the decay width data set), one clearly observes negligible modifications of their fit quality. Moreover, the  $\chi^2$  obtained for the individual  $A^{sh}$ ,  $B^{sh}$ ,  $C^{sh}$  spectrum lineshapes are also quite reasonable.

The numbers shown boldface and within parentheses in the first data column are also quite interesting. Fixing the arbitrary scales to their fit values (given in second data column) for each  $\tau$  data set, one can *compute* the  $\chi^2$  distance of each of the  $A^{sh}$ ,  $B^{sh}$ ,  $C^{sh}$  spectrum lineshapes to the fit solution to *only* the  $e^+e^-$  data. Comparing these numbers to their homologues in the second column (obtained, instead, with the  $\tau$  spectrum lineshapes fitted) clearly proves that the  $e^+e^-$  data allow to *predict* the  $\tau$  spectrum lineshape with very good accuracy<sup>16</sup>. One should note that, if unconstrained, all  $\tau$  spectrum normalizations prefer consistently a rescaling by  $\simeq -5\%$ . As discussed in Subsection 3.1 above, the exact meaning of such rescalings should be considered with great care.

In Figure 4 we plot the fit residuals normalized to the fit function value, namely :

$$x_i = \frac{(1 + \lambda)m_i - f_i}{f_i} \quad , \quad i = 1, N_{Exp} \quad (15)$$

neglecting the effects of correlations on the plotted errors. This plot clearly shows that, up to  $\simeq 1$  GeV, the residuals can be considered as flat, structureless, distributions ; Figure 4 is the exact analog of Figure 12 in [17] and exhibits the similar character of BELLE and CLEO data in our fitted  $s$  range.

The last data column in Table 3 displays the fit information while fitting the  $\mathcal{B}_{\pi\pi}/N dN/ds$  distributions of the various  $\tau$  experiments together with the whole set of  $e^+e^-$  data, taking into account the constraint imposed on the  $\lambda$  scale factors by the uncertainty on the measured branching ratio values  $\mathcal{B}_{\pi\pi}$ .

The full fit thus obtained is also quite satisfactory as reflected by the fit probability (80%). It shows, nevertheless, that a significant rescaling of the experimental data is requested. For the  $\tau$  data sets, the partial  $\chi^2$  information is displayed as  $x/y$  where  $x$  is the part of the  $\chi^2$  coming from the data points and  $y - x$  is the contribution of the  $(\lambda/\eta)^2$  term (see Eq. (12)).  $\sqrt{y - x}$  tells how far from the  $\mathcal{B}_{\pi\pi}$  central value – in units of  $\eta_{Exp}$  –, the spectrum normalization is preferred. Assuming no external cause to the rescaling, the numerical values of the corresponding coefficients look close to the expected  $\mathcal{B}_{\pi\pi}$  value, taking into account the reported accuracy of the various measurements. Compared to these, the fit values are found at resp.  $2.9 \sigma_{ALEPH}$ ,  $1.4 \sigma_{BELLE}$  and  $1.5 \sigma_{CLEO}$  towards lower central values for  $\mathcal{B}_{\pi\pi}$ .

The results are represented in Figures (5), (6) and (7). In Figure (6) one clearly sees that the residuals for CLEO and BELLE are consistent with those in Figure (3), while those for ALEPH exhibit a structure around the  $\rho$  peak location. We have widely discussed in Subsection 3.1 the behavior of ALEPH, BELLE and CLEO residuals under very close conditions<sup>17</sup>. Figure (7) gives another view : Comparing Figure (7) to Figure (4) shows that the residual distributions remain flat up to the  $\simeq \phi$  mass, but slightly shifted towards positive values.

<sup>16</sup>We already reached this conclusion [4] with the CLEO data sample lineshape.

<sup>17</sup>The differences between Figures 6 and 1 is essentially due to the fact that we now perform a simultaneous fit of ALEPH, BELLE and CLEO data sets instead of examining each them in isolation. In these conditions the values found for  $\delta g$  and  $\delta m^2$  are dominated by BELLE and CLEO which prefer a smaller value for  $\delta g$  than ALEPH.



Data Set (# data points)	No $\tau$ Data NSK( $e^+e^-$ )	$\tau$ Data Set Configurations	
		NSK + A <sup>sh</sup> B <sup>sh</sup> C <sup>sh</sup>	NSK + ABC
Decays (9)	14.84	15.12	16.20
New Timelike (127)	118.88	120.24	126.47
Old Timelike (82)	50.65	51.08	60.45
$\pi^0\gamma$ (86)	66.03	65.84	66.07
$\eta\gamma$ (182)	135.26	135.54	135.78
$\pi^+\pi^-\pi^0$ (126)	139.45	139.42	139.44
$\delta g$	—	<b>0</b>	$[-0.30 \pm 0.07] 10^{-1}$
$\delta m^2$ (GeV <sup>2</sup> )	—	<b>0</b>	$[1.06 \pm 0.62] 10^{-3}$
ALEPH (37+1)	<b>(23.52)</b>	19.23	28.30/36.51
ALEPH Scale (%)	—	$-5.45 \pm 0.62$	$-1.46 \pm 0.38$
CLEO (29+1)	<b>(35.57)</b>	31.83	37.22/39.46
CLEO Scale (%)	—	$-5.48 \pm 1.01$	$-2.60 \pm 0.54$
BELLE (19+1)	<b>(27.16)</b>	27.61	26.43/28.29
BELLE Scale (%)	—	$-4.80 \pm 0.71$	$-2.09 \pm 0.46$
$\chi^2/\text{dof}$	525.10/597	605.90/679	648.68/680
Probability	98.4%	97.9%	80.1%

Table 3: Individual  $\chi^2$  of the data samples under various fit configurations. The  $e^+e^-$  data sets are referred to in the text. Inclusion of ALEPH, BELLE and CLEO data sets are referred to in column flags as A, B and C, respectively. A<sup>sh</sup>, B<sup>sh</sup>, C<sup>sh</sup> correspond to fitting the lineshape of the normalized invariant mass spectra only. Numbers indicated boldface are the  $\chi^2$  distances of A<sup>sh</sup>, B<sup>sh</sup>, C<sup>sh</sup> to the fit solution of *only* the  $e^+e^-$  data. Parameter values written boldface are not allowed to vary in fits.

The error covariance matrix of the fit parameters still exhibits some large correlations as  $(g, \delta g) \simeq 40\%$  and  $(g, \delta m^2) \simeq (\delta g, \delta m^2) \simeq -40\%$ . One also gets correlations at the +20% level between  $\lambda_{ALEPH}$ ,  $\lambda_{BELLE}$  and  $\lambda_{CLEO}$ , while all others do not exceed a few percent level.

The sign of the correlations for  $(g, \delta m^2)$  and  $(\delta g, \delta m^2)$  prevents a possible relation of the form  $m^2 + \delta m^2 = a[g + \delta g]^2 f_\pi^2$  for the  $\rho^\pm$  mass squared. Relying on the global fit of all  $\tau$  data samples, one gets :

$$\left\{ \begin{array}{l} \frac{\Gamma_{\rho^\pm} - \Gamma_{\rho^0}}{\Gamma_{\rho^0}} \simeq \frac{2\delta g}{g} = [-1.10 \pm 0.26] \% \\ m_{\rho^\pm}^2 - m_{\rho^0}^2 = \delta m^2 = (1.06 \pm 0.62) 10^{-3} \text{ GeV}^2 \end{array} \right. \quad (16)$$

significantly smaller than for ALEPH only (see Eq. (13)). In this case, the mass difference between the two  $\rho$  mesons is  $m_{\rho^\pm} - m_{\rho^0} \simeq 0.68 \pm 0.39$  MeV, whereas  $\Gamma_{\rho^\pm} - \Gamma_{\rho^0} \simeq -1.63 \pm 0.39$  MeV only.

Summarizing the results gathered in Table 3, one can conclude that  $e^+e^-$  data and  $\tau$  data do not exhibit inconsistencies. Indeed, the fit of the spectra reported in the third data column is quite satisfactory, and this takes into account all reported experimental information. This agreement at the the form factor level, does not *a priori* mean that similar  $g - 2$  values will be obtained when using/removing  $\tau$  data.

Taking into account the statistical significance of the rescaling factors as reflected by their uncertainties (see Table 3), we neglect none of them in the rest of this analysis. One may stress once again that these rescaling factors may well only reflect an incomplete account of the isospin breaking effects affecting the  $\tau$  spectra lineshape which have to be "subtracted" in order to compute estimates of the  $\pi\pi$  loop contribution to  $g - 2$ .

Finally, one may also wonder to reach as frequently such favorable probabilities. As can be seen in Table 3, this reflects the low contributions to the  $\chi^2$  yielded by the old  $\pi\pi$  data [49, 51] ( $\chi^2/n \simeq 0.6$ ) and by the (recent)  $e^+e^- \rightarrow (\pi^0/\eta)\gamma$  data [38, 39, 35, 36, 37, 40] ( $\chi^2/n \simeq 0.75$ ). Instead, the newly collected  $\pi\pi$  data sets [19, 20, 21] yield  $\chi^2/n \simeq 0.9$  and the 3-pion data [19, 43, 44, 45, 41, 42]  $\chi^2/n \simeq 1.1$ , quite comparable to CLEO data  $\chi^2/n \simeq 1.3$ . Discarding the contribution of the scale penalty terms, BELLE data yield  $\chi^2/n \simeq 1.4$  and ALEPH  $\simeq 0.9$ . Therefore, these high probabilities reveal certainly some overestimation of systematic errors in definite  $e^+e^-$  data sets. When data sets for  $e^+e^- \rightarrow (\pi^0/\eta)\gamma$  with better estimated errors will become available, this question will be naturally solved ; awaiting this, one may conclude that the most precise pieces of information provided presently by the full  $e^+e^- \rightarrow (\pi^0/\eta)\gamma$  cross sections are essentially the partial widths for  $\rho^0/\omega/\phi \rightarrow (\pi^0/\eta)\gamma$ .

On the other hand, this explains why one should carefully control that some inconsistency in the fit is not hidden by these favorable probabilities. A good criterium is certainly provided by the  $\chi^2/n$  value associated with each data set and by its behavior while modifying the data set collection submitted to fit.

## 4 Consequences for the Hadronic Contribution to $g - 2$

An important outcome of our model and of our treatment of the data sets – *i.e.* our fitting procedure – is related with the estimate of hadronic contributions to  $g - 2$  up to 1 GeV. Mixing different processes correlated by the same underlying physics cannot be successful without some clear understanding of the errors in each data set, which should be properly implemented inside the fitting code. Our procedure relies on the whole available information on uncertainties

(magnitude and type). This allows us to draw conclusions directly from a global fit to several data sets rather than combining physics information derived from separate fits to the individual data samples.

However, this does not guarantee that combining various experiments will result in improved uncertainties. Indeed, the way the systematic errors, especially scale uncertainties, combine in the fit procedure cannot be straightforwardly guessed. One may, nevertheless, expect the results to be more reliable ; indeed, assuming systematics are randomly distributed, the net result of mixing different experiments and/or data sets should be to neutralize them to a large extent<sup>18</sup>.

The lowest order contribution of a given annihilation process  $e^+e^- \rightarrow H$  to the muon anomalous magnetic moment  $a_\mu = (g - 2)/2$  is given by :

$$a_\mu(H) = \frac{1}{4\pi^3} \int_{s_H}^{s_{cut}} ds K(s) \sigma(s) \quad (17)$$

where  $\sigma(s)$  is the Born cross section of the annihilation process  $e^+e^- \rightarrow H$ ,  $s_H$  its threshold squared mass and  $s_{cut}$  is an assumed end point of the non-perturbative region.  $K(s)$  is a known kernel [13] given by the integral :

$$K(s) = \int_0^1 dx \frac{x^2(1-x)}{x^2 + (1-x)s/m_\mu^2} \quad , \quad (18)$$

$m_\mu$  being the muon mass. For  $s > 4m_\mu^2$ , this writes :

$$\left\{ \begin{array}{l} K(s) = \frac{x^2}{2}(2-x^2) + \frac{(1+x^2)(1+x^2)}{x^2} \left[ \ln(1+x) - x + \frac{x^2}{2} \right] + \frac{1+x}{1-x} x^2 \ln x \\ \text{with : } x = \frac{1-\beta}{1+\beta} \quad \text{and} \quad \beta = \sqrt{1 - \frac{4m_\mu^2}{s}} \end{array} \right. \quad (19)$$

and, for  $0 < s \leq 4m_\mu^2$ , it becomes [13] ( $r = s/m_\mu^2$ ) :

$$K(s) = \frac{1}{2} - r + \frac{1}{2}r(r-2) \ln r - (1-2r + \frac{r^2}{2}) \sqrt{\frac{r}{4-r}} \arctan \sqrt{\frac{4-r}{r}} \quad (20)$$

This expression has to be used in order to integrate the cross section for  $e^+e^- \rightarrow \pi^0\gamma$  below the two-muon threshold.

Our global fit provides the theoretical Born cross sections with their parameter values, errors and their (full) covariance matrix. As illustrated above and in [1], the results obtained while fitting altogether several  $e^+e^-$  cross sections and  $\tau$  spectra are satisfactory. Therefore, we consider that using our cross sections within a Monte Carlo, which fully takes into account the parameters, their errors and correlations, should provide a fairly well motivated value for each accessible  $a_\mu(H)$  in our fitting range (*i.e.* from each threshold up to  $\simeq 1$  GeV/c) and for its uncertainty which appropriately merges statistical and systematic errors.

---

<sup>18</sup> Of course, one cannot completely exclude that systematics could "pile up" coherently ; however, if the number of different data sets is large enough, such a possibility looks rather unlikely.

In order to allow for a motivated comparison between our results and experimental estimates for  $a_\mu(\pi^+\pi^-)$ , one should also include the effects of Final State Radiation (FSR) into our estimates of the  $\pi\pi$  contribution to the muon anomalous moment. Indeed, even if not always manifest, the shift produced by FSR corrections is included in the reported [19, 20, 21] experimental values for  $a_\mu(\pi^+\pi^-)$ . The FSR corrections are accounted for by multiplying the  $\pi\pi$  Born cross section in Eq. (17) by [13] :

$$1 + \eta_{FSR}(s) = \left(1 + \eta(s) \frac{\alpha_{em}}{\pi} - \frac{\pi\alpha_{em}}{2\beta}\right) \frac{\pi\alpha_{em}}{\beta} \left(1 - \exp\left\{-\frac{\pi\alpha_{em}}{\beta}\right\}\right) \quad (21)$$

where the Schwinger function[52]  $\eta(s)$  can be found corrected for a missprint in [53] together with a simplified expression (also derived by Schwinger) valid at the 1.5% level. The uncertainties affecting the FSR effect estimates are not known ; nevertheless, they are expected small in our range of interest[13] ; we, therefore, neglect their contribution to the errors we report on  $a_\mu(\pi\pi)$ . Finally, FSR effects on contributions other than  $\pi\pi$  to  $a_\mu$  are also known to be negligible [13] and are thus neglected.

## 4.1 Global Fit Results And $e^+e^-$ Data

It is quite important to compare the outcome of our model and fit procedure with experimental data. This should allow to check for possible methodological biases and to substantiate how the merging of statistical and systematic errors operates.

CMD-2 [19, 20] and SND [21], for instance, have published  $a_\mu(\pi^+\pi^-)$  obtained by integrating numerically their measured  $e^+e^- \rightarrow \pi^+\pi^-$  cross section over the interval  $\sqrt{s} = 0.630 \div 0.958$  GeV, using the trapezoidal method. We have run our code using separately each of the data sets given in resp. [19], [20] and [21] together with the relevant set of decay partial widths of vector mesons needed in order to determine numerically the SU(3)/U(3)/SU(2) breaking parametrization.

The results are given in the upper part of Table 4 and look in good correspondence with expectations. The highly favorable probability for the SND spectrum [21] might be attributable to its larger systematics compared to CMD-2. The middle line in this Table shows the result obtained while fitting simultaneously the three Novosibirsk spectra [19, 20, 21] together. The global fit of these data sets, where systematics are certainly under good control, provides a strong reduction of the global uncertainty – merging all reported systematic and statistical errors. The improvement of the uncertainty derived from the global fit solution compares favorably with the average value proposed by [14] using a spline method. Therefore, nothing obviously abnormal is recognized in this comparison. The following line shows that KLOE data [54] allows to reduce a little bit more the uncertainty ; both the central value and the uncertainty compare well with the average proposed by [14]. However, one should note the very low probability of the associated global fit.

The next three lines in Table 4 are also quite interesting. The first of these reports the result obtained when fitting using all available  $\pi^+\pi^-$  data sets – except for KLOE [18] ; this turns out to include into the fitted data the so-called "Old Timelike Data" [49, 51] (82 measurements) besides the "New Timelike Data" (127 measurements). The central value for  $a_\mu(\pi\pi)$  is slightly shifted downwards by about  $1\sigma$  with a negligible gain in precision. One also observes that the fit probability makes a large jump ( $\simeq 50\% \Rightarrow \simeq 90\%$ ), reflecting the larger uncertainties in

Data Set	Experimental Result	Fit Solution	Statistical Information	
			$\chi^2/\text{dof}$	Probability
CMD-2 (1995)	$362.1 \pm (2.4)_{stat} \pm (2.2)_{syst}$	$362.57 \pm 2.64$	42.46/44	53.8%
CMD-2 (1998)	$361.5 \pm (1.7)_{stat} \pm (2.9)_{syst}$	$362.36 \pm 2.14$	38.05/40	55.9%
SND (1998)	$361.0 \pm (1.2)_{stat} \pm (4.7)_{syst}$	$361.09 \pm 2.04$	27.10/46	98.8%
NSK New Timelike $\pi^+\pi^-$	$360.0 \pm 3.02_{exp} \quad ***$	$361.39 \pm 1.72$	124.61/128	56.8%
NSK New Timelike $\pi^+\pi^- + \text{KLOE}$	$358.5 \pm 2.41_{exp} \quad ***$	$360.25 \pm 1.48$	255.22/188	0.1%
NSK( $\pi^+\pi^-$ )		$359.50 \pm 1.60$	180.09/210	93.3%
NSK ( $\pi^+\pi^-$ ) + ( $\pi^0/\eta$ ) $\gamma$		$359.42 \pm 1.52$	373.59/468	99.96%
NSK ( $\pi^+\pi^-$ ) + ( $\pi^0/\eta$ ) $\gamma$ + ( $\pi^+\pi^-\pi^0$ )		$359.31 \pm 1.62$	525.10/597	98.4%

Table 4: Contributions to  $10^{10}a_\mu(\pi\pi)$  from the invariant mass region  $0.630 - 0.958 \text{ GeV}/c$ . The data flagged by  $***$  are combined values proposed in [14] for the New Timelike data altogether, with or without KLOE data [54]. The first three lines in this Table refer to  $a_\mu(\pi\pi)$  experimental values given in resp. [19], [20] and [21]. "NSK ( $\pi^+\pi^-$ )" indicate that *all* annihilation data to  $\pi^+\pi^-$  are considered.

the data from [49, 51] compared to those from [19, 20, 21]. This once more shows that the systematics in the data sets from [49, 51] have been conservatively estimated.

The last 2 lines in Table 4 exhibit the same trend ; indeed, including in the fit procedure the 86 measurements of  $e^+e^- \rightarrow \pi^0\gamma$ , the 182 measurements of  $e^+e^- \rightarrow \eta\gamma$  and the 126 points of  $e^+e^- \rightarrow \pi^0\pi^+\pi^-$  from [19, 43, 44, 45, 41, 42] does not improve, strictly speaking, the uncertainty ; however, it is satisfactory to check that the central value only fluctuates inside quite acceptable limits. This teaches us some remarkable facts :

- Improving systematics in all processes having the same underlying physics as  $\pi^+\pi^-$  might be useful to allow a better determination of their own contributions to  $a_\mu$ , but also of  $a_\mu(\pi\pi)$  itself. Indeed, most physics parameters in the quoted processes are the same as in  $e^+e^- \rightarrow \pi^+\pi^-$ . Conversely, higher quality  $\pi^+\pi^-$  data should improve estimating the contributions of the other related annihilation processes to  $a_\mu$ .
- If errors are reasonably well understood and appropriately dealt with, adding poor quality data sets into the fitted sample does not degrade the result ; this allows, however, to

confirm the stability of the central values, which is certainly a valuable piece of information.

However, the most important remark is certainly that using the radiative partial width decays of light mesons – and/or the  $e^+e^- \rightarrow (\pi^0/\eta)\gamma$  cross sections – together with  $e^+e^- \rightarrow \pi^+\pi^-$  allows a quite significant improvement of the accuracy on  $a_\mu(\pi\pi)$  compared to the direct numerical integration of the experimental spectra. This is, indeed, the main advantage of having a constraining global model allowing for an overconstrained global fit.

## 4.2 Effects Of Including $\tau$ Spectra And KLOE Data

One may question the effects produced by introducing the  $\tau$  decay data inside our collection of fitted data sets. These are expected to improve the model parameter values (and errors), if their systematics are indeed reasonably well controlled.

Our strategy will be to consider all  $e^+e^-$  data sets used just above and look at the effect of including the A [15], B [17] and C [16] data samples in isolation or combined.

As above, when using the fit results obtained by constraining the rescaling factors – *i.e.* keeping the  $(\lambda/\eta)^2$  terms in the  $\chi^2$  expressions for  $\tau$  data samples – the  $\tau$  samples will be denoted A, B and C ; when concentrating over  $\tau$  lineshapes, these will be denoted  $A^{sh}$ ,  $B^{sh}$  and  $C^{sh}$ . The case when fitting the  $\tau$  spectra by allowing non-vanishing  $\delta g$  and  $\delta m^2$  and imposing  $\lambda \equiv 0$  will still be referred to as  $A_{dm,dg}$ ,  $B_{dm,dg}$  or  $C_{dm,dg}$  in our Tables and/or Figures.

### 4.2.1 Comparison With Standard $\tau$ Based Estimates for $a_\mu$

When letting free  $\delta g$  and  $\delta m^2$  while imposing  $\lambda \equiv 0$ , our approach is comparable to those underlying the so-called  $\tau$  based estimates [14] of the hadronic contribution to the muon  $g - 2$ . Indeed, the whole set of  $e^+e^-$  data fixes in a data driven mode all identified isospin breaking corrections :  $\rho - \omega$  and  $\rho - \phi$  meson mixing,  $\rho$  meson mass and width differences, I=0 part of the  $\rho$  revealed by its coupling to photon<sup>19</sup> (see Eq. (14)) and FSR corrections. The pion mass difference is plugged in directly. It is thus interesting to compare our results in this case with the existing estimates and thus check the effects of a global fit. The hadronic contributions to the muon  $g - 2$  derived from  $\tau$  data have been updated recently in [14] ; the numerical contributions to  $a_\mu$  from the reference region  $\sqrt{s} \in [0.63, 0.958]$  are not published but have been kindly communicated to us [55].

Table 5 displays the experimental data derived from each existing  $\tau$  data set and their combination [14, 55] in the first data column. One may note that the proposed experimental average is larger than each of the individual estimates ; actually, in order to perform the average, each individual estimate has been rescaled to the world average value for  $\mathcal{B}_{\pi\pi}$  [55]. The total (experimental) errors displayed are computed by summing up the various components in quadrature. This is provided in order to allow for an easy comparison with our fit result. The data columns  $\chi_\tau^2/\text{dof}$  and  $\chi_{ee}^2/\text{dof}$  display the contribution to the total  $\chi^2$  provided by resp. the  $\tau$  and the so-called New Timelike  $e^+e^-$  annihilation data [19, 20, 21], which serve as quality tags.

---

<sup>19</sup>This contribution is currently not considered as such [14]. It should be partly absorbed in  $\rho$  meson width corrections.

Data Set	$a_\mu(\pi\pi)$	$a_\mu(\pi\pi)$	Statistical Information		
	Experimental Result	Fit Solution	$\chi^2_\tau/\text{dof}$	$\chi^2_{ee}/\text{dof}$	Probability
$A_{dm,dg}$ [15]	$364.02 \pm (2.19)_{exp} \pm (1.97)_{Br} \pm (1.51)_{IB}$ ( $364.02 \pm 3.31_{tot}$ )	$362.83 \pm 1.46$	45.52/37	122.12/127	95.3%
$B_{dm,dg}$ [17]	$366.44 \pm (1.02)_{exp} \pm (5.70)_{Br} \pm (1.51)_{IB}$ ( $366.44 \pm 5.98_{tot}$ )	$364.85 \pm 1.32$	41.95/19	128.58/127	76.5%
$C_{dm,dg}$ [16]	$366.62 \pm (4.17)_{exp} \pm (6.37)_{Br} \pm (1.51)_{IB}$ ( $366.62 \pm 8.05_{tot}$ )	$364.23 \pm 1.82$	63.01/29	125.63/127	70.0%
OPAL [31]	$354.40 \pm (4.67)_{exp} \pm (4.78)_{Br} \pm (1.51)_{IB}$ ( $354.40 \pm 6.85_{tot}$ )	–	–	–	–
ALL $\tau$ Sets	$367.46 \pm (1.31)_{exp} \pm (1.59)_{Br} \pm (1.51)_{IB}$ ( $367.46 \pm 2.55_{tot}$ )	$367.12 \pm 1.30$	102.06/85	143.32/127	58.2%

Table 5: Contributions to  $10^{10}a_\mu(\pi\pi)$  from the invariant mass region  $0.630 - 0.958$  GeV/c. The experimental values [55] are derived using the method from [14]. The experimental average includes OPAL data, our fit result does not. The meaning of  $A_{dm,dg}$ ,  $B_{dm,dg}$ ,  $C_{dm,dg}$  is explained in the text.

One should note the nice correspondence between our central values and the corresponding experimental estimates. The improvement of the total errors provided by the global fit method is also worth mentioning. The reduction of the uncertainties provided when using  $\tau$  data looks even more important that when using  $e^+e^-$  data alone. Of course, the errors provided there, as anywhere in this paper, are the MINUIT errors returned by the fits.

The result for  $(A_{dm,dg} B_{dm,dg} C_{dm,dg})$  – last line in Table 5 – is also quite remarkable. It clearly illustrates that our global fit does not lead to a standard averaging, but takes into account the relative mismatch of the A, B and C lineshape distortions noted in Subsection 3.1. In this procedure, the fit average is significantly pushed upwards, in accord with the experimental estimate<sup>20</sup>.

The data columns providing the  $\chi^2$  information are also quite important. As already noted in Subsection 3.1,  $\chi^2_{ALEPH}$  is reasonably good simultaneously with the New Timelike  $e^+e^-$  data. Comparing  $\chi^2_{ALEPH}$  here (45.52) with its homologue in Table 1 – fourth line therein – (29.17), reveals that the ALEPH data sample meets some difficulty in accomodating the data for  $e^+e^- \rightarrow \pi^+\pi^-\pi^0$ . However, the description remains quite reasonable and one may conclude that there is no real mismatch, within our approach, between ALEPH data and the VMD expectations. The  $a_\mu$  value just derived from ALEPH data compares well with those

<sup>20</sup> This should be slightly larger, if removing the OPAL data set [31].

derived from  $e^+e^-$  data only (see Table 4).

The values for  $a_\mu$  derived for BELLE and CLEO data in isolation, even if slightly larger than expected from VMD inference, are not in strong disagreement with these. However, as can be seen from either of Table 5 and Table 1 (see the  $\lambda \equiv 0$  entries therein), the fit quality, as reflected by  $\chi_{BELLE}^2$  and  $\chi_{CLEO}^2$  looks significantly poorer (both yield  $\chi^2/npoints \simeq 2$ ) than ALEPH ( $\chi^2/npoints \simeq 1.1 \div 1.2$ ). Whether this behavior reveals specific systematics is an open issue.

When performing the global fit with all  $\tau$  data samples (last line in Table 5), the weight of  $\tau$  data happens to become dominant. In this case, the fit of the  $\tau$  data is nearly unchanged ( $\chi_{ALEPH}^2 = 26.64$ ,  $\chi_{BELLE}^2 = 45.89$ ,  $\chi_{CLEO}^2 = 29.52$ ); however, even if apparently reasonable, the new timelike  $e^+e^-$  data yield a  $\chi_{ee}^2$  increased by 20 units, which is significantly far enough from optimum that we consider the corresponding  $a_\mu$  value with great care.

The analysis in Subsection 3.1 has shown that rescaling factors and lineshape distortions are sharply related. However, in order to derive  $\tau$  based estimates for  $a_\mu$ , one should remove all distortions produced by isospin breaking effects specific of the  $\rho^\pm$  meson relative to  $\rho^0$ . Therefore, we do not consider reliable the estimates provided in Table 5, except possibly those in the  $A_{dm,dg}$  entry, as the distortions in the B and C samples are to be better understood.

#### 4.2.2 Additional $\tau$ Based Estimates of $a_\mu$

Our analysis in Subsection 3.1 provided a serious hint that rescaling the  $\tau$  spectra can be an effective way to account for shape distortions produced by IB effects which differentiate the  $\rho^\pm$  and  $\rho^0$  mesons. We just provided results assuming no scale correction to the  $\tau$  data samples ( $\lambda_{ALEPH} = \lambda_{BELLE} = \lambda_{CLEO} = 0$ ). In order to provide a complete picture, it is worth considering two more sets of fitting conditions. In this Subsection, we will present the results derived by : i/ fitting the  $\tau$  spectrum lineshapes by the method emphasized in Subsection 2.2.2, ii/ fitting the  $\tau$  spectra by allowing non-vanishing rescalings, however, constrained by the relevant  $(\lambda/\eta_{Exp})^2$  term for each of the  $\tau$  data set.

The upmost part of Table 6 collects our results for  $a_\mu$  obtained using the  $\tau$  data samples, except for the first line which is nothing but the final result in Table 4. The second line shows that including the  $\tau$  lineshapes into the fit ( $A^{sh}$ ,  $B^{sh}$ ,  $C^{sh}$ ) gives results perfectly consistent with using only  $e^+e^-$  data and a slightly improved uncertainty. As the fit quality of each  $A^{sh}$ ,  $B^{sh}$  and  $C^{sh}$  on the one hand, and each of the  $e^+e^-$  data are simultaneously optimum, one may consider this estimate safe.

Compared with pure  $e^+e^-$  estimates, the next 3 lines show the effects of including each of A, B and C in isolation<sup>21</sup>. The  $a_\mu$  value found for ALEPH agrees with that in the  $A_{dm,dg}$  entry in Table 5. Interestingly, the values found using either B or C are significantly lower than their homologues in Table 5, but in nice correspondence with VMD expectations (see Table 4). This may indicate that some rescaling is needed for these, consistent with their uncertainties.

A simultaneous use of A, B and C (line flagged with NSK+ABC) provokes an upward shift by  $4 \cdot 10^{-10}$ , as already observed in Table 5. The behavior of the combination under the fit illustrates, once again, that the shape distortions exhibited by each of A, B and C are different and that the compensation performed by the fit degrades the description of the  $e^+e^-$  data. This produces the increased value for  $a_\mu$ , as also observed in the previous Subsection.

<sup>21</sup>And keeping the  $(\lambda/\eta)^2$  term included in the  $\chi^2$  expression, as stated above.



Data Set	Fit Solution	Statistical Information	
		$\chi^2/\text{dof}$	Probability
	$10^{10}a_\mu(\pi\pi)$		
NSK ( $e^+e^-$ )	$359.31 \pm 1.62$	525.10/597	98.4%
NSK + A <sup>sh</sup> B <sup>sh</sup> C <sup>sh</sup>	$359.62 \pm 1.51$	605.90/679	97.9%
NSK + A ( $\chi_\tau^2 = 28.39$ )	$362.24 \pm 1.52$	568.60/632	96.6%
NSK + B ( $\chi_\tau^2 = 32.59$ )	$360.68 \pm 1.47$	558.88/614	94.6%
NSK + C ( $\chi_\tau^2 = 39.13$ )	$360.52 \pm 1.55$	565.24/624	95.5%
NSK + A B C	$364.48 \pm 1.34$	648.60/680	80.1 %
NSK + KLOE	$359.22 \pm 1.32$	652.92/657	51.9%
NSK + KLOE + A <sup>sh</sup> B <sup>sh</sup> C <sup>sh</sup>	$358.52 \pm 1.32$	741.50/739	46.7%
NSK + KLOE + A B C	$364.04 \pm 1.25$	792.28/740	8.9%
NSK + KLOE + A ( $\chi_\tau^2 = 49.59$ )	$361.55 \pm 1.31$	708.90/692	32.0%
NSK + KLOE + B ( $\chi_\tau^2 = 34.06$ )	$360.19 \pm 1.16$	688.02/674	34.6%
NSK + KLOE + C ( $\chi_\tau^2 = 39.89$ )	$360.11 \pm 1.32$	693.40/684	39.3%

Table 6: Contributions to  $10^{10}a_\mu(\pi\pi)$  from  $\sqrt{s} \in [0.630, 0.958]$  GeV/c.  $\tau$  data set configurations are considered together with the  $e^+e^-$  data and the appropriate subset of decay partial widths. The meaning of A, B, C, and A<sup>sh</sup>, B<sup>sh</sup>, C<sup>sh</sup> is given in the text. The contribution of single  $\tau$  subsets to the total  $\chi^2$  is indicated when relevant by ( $\chi_\tau^2 = \dots$ ). For lineshape fits without KLOE data, we have  $\chi_\tau^2 = 18.22$  for A,  $\chi_\tau^2 = 28.35$  for B and  $\chi_\tau^2 = 31.88$  for C.

### 4.2.3 Including KLOE Data

Up to now, we have not introduced the KLOE [18] data into the data sets submitted to a fit. Indeed, even if considered acceptable, its best  $\chi^2/n_{points}$  looks large [1]. It is nevertheless instructive to point out explicitly its effects. Table 2 in [1] indicates that three among the rescaling coefficients can be cancelled out ; one only has to let vary those corresponding to the global scale ( $\varepsilon_0$ ) and to the acceptance correction ( $\varepsilon_2$ ) [18].

This provides the results given in the lower half of Table 6. Even if the probability decreases due to the intrinsically high (minimum)  $\chi^2$  of the KLOE data sample, one observes a good consistency of the  $a_\mu(\pi\pi)$  value derived from fitting the (rescaled) KLOE data together with all  $e^+e^-$  Novosibirsk data. One also starts getting much improved uncertainties. One may note the good probability when using all NSK data together with KLOE and  $A^{sh} B^{sh} C^{sh}$  and the improved uncertainties on  $a_\mu(\pi\pi)$ . When using A, B and/or C, one finally observes the same trend as in the upper part of Table 6, which lead us to be as cautious in this case.

Nevertheless, one may conclude that KLOE data do not degrade the expectations from NSK data, whatever is done with  $\tau$  data.

In order to assess the effects of a global fit, it is also interesting to compare the result for NSK+KLOE in Table 6 with the corresponding average published in [14] :

$$\text{GlobalFit} : a_\mu(\pi\pi) = 359.22 \pm 1.32 \iff \text{Average}[14] : a_\mu(\pi\pi) = 358.51 \pm 2.41_{exp}$$

in units of  $10^{-10}$ . As for NSK data alone, the central value from our fit is slightly larger than the estimate from [14] and the uncertainty is significantly improved.

#### 4.2.4 A Partial Summary

In summary, the picture exhibited when using the  $\tau$  data samples looks somewhat intricate. We have shown above, especially in Subsection 3.1, that lineshape distortions and absolute scale of spectra are intimately related.

However, the present analysis tends to indicate that an important part of the reported discrepancy between  $e^+e^-$  and  $\tau$  based estimates of  $g - 2$  is related with a more or less difficult way to account for isospin breaking effects differentiating the  $\rho^\pm$  and  $\rho^0$  lineshapes. This conclusion is enforced by comparing the behavior of the ALEPH data set with those of BELLE and CLEO : the distortions of the former set can be accounted for within our model, providing a reasonable accord with VMD expectations.

As for BELLE and CLEO, genuine mass and width differences compared to  $\rho^0$ , which successfully work with ALEPH data, do not avoid a residual distortion effect which has important consequences while estimating  $a_\mu$ .

Interestingly, the normalized  $\tau$  spectra do not reveal the same problem. This is certainly due to the fact that a free rescaling allows to disconnect lineshape distortions as parametrized by mass and width differences ( $\delta g$  and  $\delta m^2$  in our model) from the absolute scale. This indicates that the distortions exhibited by BELLE and CLEO are not understood. Of course, one cannot exclude that the agreement with ALEPH is purely accidental and that a more refined IB mechanism might have to be considered.

Figure 8 displays graphically the main conclusions discussed in this Section. The vertical line centered at the value derived by fitting all Novosibirsk data is drawn to guide the eye. Comparing our estimates with the experimental data reported there is also interesting by itself. This indicates that individual estimates of  $a_\mu$  provided by each of the  $\tau$  data sets are close to the  $e^+e^-$  based estimate. The combined fit of these, instead, exhibits a clear discrepancy, as shown by the data points flagged by NSK + A+B+C, NSK +  $A_{dm,dg} + B_{dm,dg} + C_{dm,dg}$  or with KLOE. Interestingly, the comparison of the various data points exhibits the same trend.

### 4.2.5 Comments On Our Model Uncertainties

Uncertainties intrinsic to our model may have to be estimated. For this purpose, having alternative models able to cover the same scope than our extended model would be desirable. Unfortunately, such models do not seem to exist which could cope with detailed descriptions of several decay channels over our whole fitting range. Some interesting attempts have been initiated relying on Chiral Symmetry and the properties of the Roy equations [56, 57] ; however, nothing final is presently available.

In our case, one cannot make estimates by changing, for instance, the  $\rho$  parametrization (Gounaris–Sakurai, Breit–Wigner, Kuhn–Santamaria . . .) as sometimes done elsewhere. Indeed, the form factor lineshape is intrinsic to the model, including the IB vector meson mixing. However, the difference between the central values of our estimates and the corresponding experimental estimates [19, 20, 21] may give some hint on the bound for our model uncertainty.

### 4.3 Comparison with $a_\mu$ Estimates Collected by the ISR Method

As a summary, our preferred final result is derived using all  $e^+e^-$  data collected at Novosibirsk :

$$a_\mu(\pi\pi; 0.630 \div 0.958 \text{ GeV}) = [359.31 \pm 1.62_{exp}] 10^{-10} \quad (22)$$

and corresponds to an (underlying) fit probability of 98.4%.

This result can be compared with the recent estimate published by KLOE [54] :

$$a_\mu(\pi\pi; 0.630 < m_{\pi\pi} < 0.958) = (356.7 \pm 0.4 \pm 3.1) 10^{-10}$$

based on a newly collected data set [18, 58]. This estimate may look a little bit low, but is consistent with ours at  $\simeq 0.7 \sigma$  level.

On the other hand, the BaBar Collaboration has recently finalized a new data set [59], also collected using the ISR method. The contribution it provides to  $a_\mu(\pi\pi)$  in the canonical  $s$  interval can be found in [60] :

$$a_\mu(\pi\pi; 0.630 \div 0.958 \text{ GeV}) = (365.2 \pm 1.9 \pm 1.9) 10^{-10} = (365.2 \pm 2.7_{tot}) 10^{-10}$$

which supersedes a preliminary result presented at the Novosibirsk Conference TAU08[61] ( $a_\mu(\pi\pi) = (369 \pm 0.8 \pm 2.9) 10^{-10}$ ). Even if larger than Eq. (22), this estimate is consistent with ours at the  $1.9 \sigma$  level.

Comparing our result with these recent estimates clearly illustrates the advantage of introducing information beyond the  $e^+e^- \rightarrow \pi^+\pi^-$  cross section and a framework which encompasses annihilation processes and partial width decays of light mesons. Indeed, the IB schemes needed can be calibrated consistently on the data set. The fact that the HLS framework does not presently go much beyond the  $\phi$  mass region is certainly a handicap, but does not prevent interesting improvements.

### 4.4 Contributions to $a_\mu$ Up To 1 GeV

The discussion above leads us to consider the best motivated results for  $a_\mu$  as derived from fit to the Novosibirsk  $e^+e^-$  data samples taking into account the photon hadronic VP (see Eq.

(36) in[1]). A challenging choice might be to include the  $\tau$  *normalized* spectra, which have been shown to yield a satisfactory description simultaneously with all  $e^+e^-$  data. We have seen that BELLE and CLEO seem to meet problems with their shape distortions which are not clearly identified. However, as  $A_{\delta m, \delta g}$  is reasonably well understood, one may consider its results for  $a_\mu$ .

Using these data samples, one can estimate several contributions<sup>22</sup> to  $a_\mu$  up to 1 GeV. They are given in Table 7. We thus provide the results obtained while fitting without any  $\tau$  sample in the first data column. The last data column, instead, shows the influence of KLOE data [18, 58].

Process	NSK (no $\tau$ )	NSK + $A^{sh} B^{sh} C^{sh}$	NSK + $A_{\delta m, \delta g}$	NSK + KLOE + $A^{sh} B^{sh} C^{sh}$
$\pi^+\pi^-$	$492.02 \pm 2.24$	$491.66 \pm 1.98$	$496.20 \pm 1.85$	$492.24 \pm 1.79$
$\pi^0\gamma$	$4.53 \pm 0.04$	$4.53 \pm 0.04$	$4.55 \pm 0.04$	$4.51 \pm 0.05$
$\eta\gamma$	$0.17 \pm 0.01$	$0.17 \pm 0.01$	$0.17 \pm 0.01$	$0.17 \pm 0.01$
$\eta'\gamma$	$0.01 \pm 0.00$	$0.01 \pm 0.00$	$0.01 \pm 0.00$	$0.01 \pm 0.00$
$\pi^+\pi^-\pi^0$	$36.99 \pm 0.55$	$36.97 \pm 0.56$	$36.83 \pm 0.56$	$37.07 \pm 0.55$
Total	$533.72 \pm 2.32$	$533.34 \pm 2.07$	$537.76 \pm 2.08$	$534.01 \pm 1.90$
Fit Probability	98.4%	98.0%	95.3%	50.8%

Table 7: Contributions to  $10^{10}a_\mu$  from thresholds up to 1 GeV/c for various processes fitting the data sets indicated on the first line ; by NSK we mean the set of all  $e^+e^-$  data except for KLOE. The errors provided merge the reported statistical and systematic uncertainties.

One can note that the estimate based only on  $e^+e^-$  annihilation data is consistently improved by including within the fitted data sets the  $\tau$  lineshapes from ALEPH, BELLE and CLEO. Instead, using  $A_{\delta m, \delta g}$  produces a shift by 4 units, while reducing the uncertainty in the same way than the  $\tau$  lineshapes. Whether this estimate should be preferred, is an open question, awaiting a better understanding of the  $\tau$  spectrum distortions. On the other hand, including KLOE data does not provokes differences with using only the Novosibirsk data, but instead provides improved uncertainties.

The always (negligible) contribution of the annihilation process  $\eta'\gamma$  is a prediction which is entirely determined by the  $\eta\gamma$  decay channel and our model which implies a tight correlation between the  $\eta\gamma$  and  $\eta'\gamma$  final states [1]. So close to its threshold, this contribution could have been expected small ; it should become obviously larger while including the  $\phi$  region.

<sup>22</sup>Actually, one could have produced, as well, these contributions up to about 1.05 GeV/c in order to include the  $\phi$  region. As our fitted region includes the  $\phi$  peak, our results would be as reliable. However, the largest ( $K\bar{K}$ ) contribution involving the  $\phi$  region is presently left aside because of the issue raised by [5] and still unsolved.

As a final remark, one may conclude that the global fit method indeed performs as expected. Moreover, as far as we know, our method is the first one which can associate a probability to the various reported contributions to the muon anomalous magnetic moment. Of course, the quoted probabilities refer to the fits underlying the estimates and not the estimates themselves, as these are only derived from computations using the fit results (parameter values and full error covariance matrix). One may infer that our preferred numerical results for  $a_\mu$  – any of the first two data columns in Table 7 – should increase the discrepancy between the prediction and the BNL measurement of the muon  $g - 2$ . Improved estimates can be expected from using also the new data samples based on the ISR method collected by KLOE and BaBar.

## 5 Summary And Concluding Remarks

In the first part of this study [1], we defined the Extended HLS Model and reminded the mechanisms implementing U(3)/SU(3)/SU(2) symmetry breaking, noticeably the vector meson mixing provided by breaking Isospin symmetry. This was shown to provide a satisfactory simultaneous description of all  $e^+e^-$  data sets considered. The annihilation channels successfully covered ( $\pi^+\pi^-$ ,  $\pi^0\gamma$ ,  $\eta\gamma$  and  $\pi^0\pi^+\pi^-$ ) represent a large amount of data. It is also the largest set of annihilation channels simultaneously analyzed so far. The present work confirms that the dipion spectrum in  $\tau$  decay is also in the reach of this model.

The  $\tau$  data sets collected by the ALEPH, BELLE and CLEO Collaborations have been carefully examined in isolation and combined within the context of a global fit performed together with a large set of  $e^+e^-$  annihilation data. For this purpose, we found appropriate to introduce additional Isospin breaking (IB) effects providing distortions of the  $\rho^\pm$  lineshape compared to  $\rho^0$ . This was partly considered in our former study [4], but totally ignored in preliminary versions of the present work like [62]. This additional mechanism (IB shape distortions) consists of a coupling difference  $\delta g$  of the  $\rho^\pm$  and  $\rho^0$  to a pion pair and a mass difference  $\delta m^2$  between these two mesons.

Each of the ALEPH (A), BELLE (B) and CLEO (C) experiments reports on a global scale uncertainty for their dipion spectra. This scale uncertainty is much smaller for A (0.51%) than for B (1.53%) or C (1.75%). The absolute scale of each  $\tau$  spectrum can then be modified by a factor  $1 + \lambda_{A/B/C}$ , including a fit parameter constrained, for each of A, B and C, by its scale uncertainty. However, it has been proved that, in minimization procedures,  $\delta g$ ,  $\delta m^2$  and these scales are tightly correlated. Therefore, one cannot interpret  $\lambda_{A/B/C} \neq 0$  as purely reflecting biases on the measured branching ratios  $\mathcal{B}(\tau \rightarrow \pi^\pm\pi^0\nu) \equiv \mathcal{B}_{\pi\pi}$ . To be explicit, the connection between pure lineshape distortion parameters and absolute scale, which is the subject of Subsection 3.1, prevents to tag reliably an undoubtful numerical value for some rescaling.

It has been shown – see Table 1 – that the ALEPH data are in accord with VMD expectations, provided some shape distortions ( $\delta g$ ,  $\delta m^2$ ) are implemented. In this case,  $\lambda_A = 0$  is even found quite acceptable. This means that, relying on ALEPH data only, the presently accepted value for  $\mathcal{B}_{\pi\pi}$  is not contradicted by our analysis. This result is tightly connected with the fact that the lineshape distortions of the ALEPH spectrum is well accounted for by our parametrization ( $\delta g$ ,  $\delta m^2$ ).

The picture is not that clear with BELLE and CLEO, indicating that some residual problem

survives, mostly visible in these data sets ; this could well be due to having a too simple-minded shape distortion mechanism ; however, this could also reflect specific systematics in these experiments or, as well, a real physical problem revealed by their larger statistics. A rescaling of their  $\mathcal{B}_{\pi\pi}$  downwards is found, however, in reasonable accord with their reported uncertainties.

Moreover, the *lineshapes* of the normalized spectra provided by A, B and C happen to exhibit no problem at all when fitted together with the largest possible set of  $e^+e^-$  annihilation data. This is certainly due to having dropped out the correlation between absolute scale and lineshape distortions. In this case, one even finds no need to introduce significant IB shape distortions. The  $\tau$  lineshapes and the  $e^+e^-$  are optimally fitted as clear from the individual  $\chi^2$  given in Table 3.

Collecting all pieces of information in this study, one cannot consider the existence of a fundamental issue, at the pion form factor level, between  $e^+e^-$  and  $\tau$  data. Indeed, Table 3, which summarizes our simultaneous description of  $e^+e^-$  annihilation and  $\tau$  decay data, displays a fit quality of about 80% with quite acceptable parameter values. This may imply as well that  $\mathcal{B}_{\pi\pi}$  is slightly overestimated or that some additional systematics affect the  $1/NdN/ds$  spectrum in some experiments.

The most important aim of the present work was to study the effects of a global fit on the estimation of hadronic contributions to  $a_\mu$ , the muon  $g - 2$ , from the various thresholds up to 1 GeV. For this purpose, our treatment of statistical and systematic errors accounted as closely as possible for the information provided for each data sample.

One first has checked that the fit performs as one could expect on individual  $e^+e^- \rightarrow \pi^+\pi^-$  data samples. Comparing our fit results with individual experimental information [19, 20, 21] about the contribution of the reference region (0.630, 0.958) GeV to  $a_\mu(\pi^+\pi^-)$  is already interesting : Table 4 shows the information returned by the fits is in good agreement with the corresponding experimental information. Performing the global fit with these data samples, where systematics have certainly been considered with great care, provides quite reasonable central values for the individual estimates of  $a_\mu(\pi^+\pi^-)$  and shrunked uncertainties ; this shrinking becomes noticeable when fitting simultaneously all  $e^+e^-$  data from [19, 20, 21] : The uncertainty is reduced from 3.02 to 1.72 in units of  $10^{-10}$ , *i.e.* better than a 40 % improvement.

The next step was to include the older  $e^+e^- \rightarrow \pi^+\pi^-$  data samples [49, 51], where systematics are certainly not as well controlled as in [19, 20, 21]. One thus gets a shift  $\Delta a_\mu(\pi^+\pi^-) \simeq -1.9$  (in units of  $10^{-10}$ ) while leaving the uncertainty nearly unchanged. Including also all the  $e^+e^- \rightarrow (\pi^0/\eta)\gamma$  and  $e^+e^- \rightarrow \pi^0\pi^+\pi^-$  data samples does not produce significant modifications, showing that the effects of systematics when combining data samples of various qualities may prevent improvements. However, the corresponding combined fit does not degrade the information ; it rather allows to check the stability of the estimate. The final uncertainty improvement is at the level of 46 %.

At this point where all information on  $e^+e^-$  annihilations – except for KLOE ISR data – are considered, one ends up with :

$$a_\mu(\pi^+\pi^-; 0.630 \div 0.958) = 359.31 \pm 1.62$$

(in units of  $10^{-10}$ ) where the error combines systematic and statistical uncertainties and accounts for the sample-to-sample correlations. The probability of the underlying fit to the data

is 98.4%. One has shown that these high probability values are a normal consequence of too conservative estimates of systematics into given data sets. This has been shown not to hide bad descriptions of some data subsets.

Including KLOE data does not modify the picture, except for the probabilities which may become very low, reflecting the intrinsic large minimum  $\chi^2$  for this data set.

Adding the various  $\tau$  data to the set of  $e^+e^-$  data samples, is also worth being made step-wise, in order to substantiate problems and specific properties of each of the A (ALEPH), B (BELLE) and C (CLEO) data sets. We have first compared (see Table 5) our reconstructed values for  $a_\mu$  with the  $\tau$  based estimates of [14] for the reference region  $0.630 \div 0.958$  GeV [55]. The central values are found in agreement while the uncertainties are importantly shrunk. This is clearly an effect of our global fit/modelling. One should also note that the parameters provided by the simultaneous fit to A, B, C and the  $e^+e^-$  data provides a value for  $a_\mu$  larger than for each of A, B and C separately. Interestingly, this property is also exhibited by the combined experimental estimate proposed by the authors of [14, 55].

In this case, we show that introducing the A, B and C lineshapes inside our fit procedure allows to confirm the value for  $a_\mu(\pi^+\pi^-; 0.630 \div 0.958)$  derived using only  $e^+e^-$  data and some more shrinking of its uncertainty :

$$a_\mu(\pi^+\pi^-; 0.630 \div 0.958) = [359.62 \pm 1.51] 10^{-10} .$$

Using additionally the KLOE data leads to :

$$a_\mu(\pi^+\pi^-; 0.630 \div 0.958) = [358.52 \pm 1.32] 10^{-10} .$$

Both results correspond to good probabilities of the underlying form factor fits.

However, our study leads us to conclude that some distortions of the lineshape, different for A and B/C, are at work which still need to be understood. Whether one is faced here with an incomplete IB distortion modelling, with unaccounted for systematics, or with some external physical effect, is an open issue. Until this issue is clarified, going much beyond the  $\tau$  lineshapes for  $a_\mu(\pi^+\pi^-)$  estimates looks hazardous.

Our results concerning  $a_\mu(\pi^+\pi^-; 0.630 \div 0.958)$  are summarized in Figure 8. This clearly illustrates that shape distortions and systematics are not completely understood, even if at the form factor level the picture is more optimistic ; this shows that  $a_\mu$  estimates are a more sensitive probe to differences than fit probabilities of the underlying form factors.

Our tendency for now is to prefer providing our final results concerning the various contributions to  $a_\mu$  from thresholds to 1 GeV, considering all NSK  $e^+e^-$  data samples together with  $\tau$  lineshape data. The KLOE data set does not seem to modify the picture unreasonably. This information is the matter of Table 7.

One may also conclude that the global fit method performs as could be expected and is a useful tool in order to examine the consistency of various data sets covering various processes related by physics. As a tool, it also permits improved estimates of the various hadronic contributions to the muon  $g - 2$ .

For this purpose, one should stress that better data, with better controlled systematics in all decay channels, and not only for the  $\pi^+\pi^-$  final state, may be valuable. Indeed, the physics correlations between the various final states in  $e^+e^-$  annihilations may conspire (better than presently) with each other in order to provide improved values for all contributions.

Theoretical developments on the inclusion of scalar mesons and higher mass vector mesons within VMD-like frameworks are also desirable, as this could increase the underlying physics correlations between the various final states accessible in  $e^+e^-$  annihilations. Finally, understanding the issue raised by [5] about the coupling of the  $\phi$  meson to  $K\bar{K}$  pairs, may well be an important task in order to estimate reliably the  $\phi$  region contribution to the muon  $g - 2$ .

## Acknowledgments

We are indebted to H. Hayashii, Nara Women's University, Nara, Japan, for having provided us with the BELLE data sample and for information concerning the BELLE Collaboration fits. We also thank Z. Zhang, LAL Orsay, to have provided us with some interesting unpublished results quoted in the text. Finally, M.B. gratefully acknowledges several useful discussions and mail exchanges with S. Eidelman, Budker Institute, Novosibirsk, Russia.

## References

- [1] M. Benayoun, P. David, L. DelBuono, and O. Leitner, Eur. Phys. J. C **C65**, 211 (2010), hep-ph/0907.4047, A Global Treatment of VMD Physics Up to To the  $\phi$  : I.  $e^+e^-$  Annihilations, Anomalies And Vector Meson Partial Widths.
- [2] M. Harada and K. Yamawaki, Phys. Rept. **381**, 1 (2003), hep-ph/0302103, Hidden local symmetry at loop: A new perspective of composite gauge boson and chiral phase transition.
- [3] T. Fujiwara, T. Kugo, H. Terao, S. Uehara, and K. Yamawaki, Prog. Theor. Phys. **73**, 926 (1985), Nonabelian Anomaly and Vector Mesons as Dynamical Gauge Bosons of Hidden Local Symmetries.
- [4] M. Benayoun, P. David, L. DelBuono, O. Leitner, and H. B. O'Connell, Eur. Phys. J. **C55**, 199 (2008), hep-ph/0711.4482, The Dipion Mass Spectrum In  $e^+e^-$  Annihilation and tau Decay: A Dynamical ( $\rho^0$ ,  $\omega$ ,  $\phi$ ) Mixing Approach.
- [5] A. Bramon, R. Escribano, J. L. L. M., and G. Pancheri, Phys. Lett. **B486**, 406 (2000), hep-ph/0003273, The ratio  $\phi \rightarrow K^+K^-/K^0\bar{K}^0$ .
- [6] G. Li, Y.-J. Zhang, and Q. Zhao, J. Phys. **G36**, 085008 (2009), 0803.3412, Study of isospin violating  $\phi$  excitation in  $e^+e^- \rightarrow \omega\pi^0$ .
- [7] Muon G-2, G. W. Bennett *et al.*, Phys. Rev. **D73**, 072003 (2006), hep-ex/0602035, Final report of the muon E821 anomalous magnetic moment measurement at BNL.
- [8] M. Davier, S. Eidelman, A. Hocker, and Z. Zhang, Eur. Phys. J. **C27**, 497 (2003), hep-ph/0208177, Confronting spectral functions from  $e^+e^-$  annihilation and tau decays: Consequences for the muon magnetic moment.



- [9] M. Davier, S. Eidelman, A. Hocker, and Z. Zhang, Eur. Phys. J. **C31**, 503 (2003), hep-ph/0308213, Updated estimate of the muon magnetic moment using revised results from  $e^+e^-$  annihilation.
- [10] M. Davier, A. Hocker, and Z. Zhang, Rev. Mod. Phys. **78**, 1043 (2006), hep-ph/0507078, The physics of hadronic tau decays.
- [11] M. Davier, eConf **C0209101**, WE03 (2002), hep-ex/0301035, Spectral functions from hadronic tau decays and QCD.
- [12] S. I. Eidelman, (2009), 0904.3275, Standard Model Predictions for the Muon  $(g - 2)/2$ .
- [13] F. Jegerlehner and A. Nyffeler, Phys. Rept. **477**, 1 (2009), 0902.3360, The Muon  $g-2$ .
- [14] M. Davier *et al.*, (2009), 0906.5443, The Discrepancy Between tau and e+e- Spectral Functions Revisited and the Consequences for the Muon Magnetic Anomaly.
- [15] ALEPH, S. Schael *et al.*, Phys. Rept. **421**, 191 (2005), hep-ex/0506072, Branching ratios and spectral functions of tau decays: Final ALEPH measurements and physics implications.
- [16] CLEO, S. Anderson *et al.*, Phys. Rev. **D61**, 112002 (2000), hep-ex/9910046, Hadronic structure in the decay  $\tau^- \rightarrow \pi^- \pi^0 \nu_\tau$ .
- [17] Belle, M. Fujikawa *et al.*, Phys. Rev. **D78**, 072006 (2008), 0805.3773, High-Statistics Study of the  $\tau^- \rightarrow \pi^- \pi^0 \nu_\tau$  Decay.
- [18] KLOE, F. Ambrosino *et al.*, Phys. Lett. **B670**, 285 (2009), 0809.3950, Measurement of  $\sigma(e^+e^- \rightarrow \pi^+\pi^-\gamma(\gamma))$  and the dipion contribution to the muon anomaly with the KLOE detector.
- [19] CMD-2, R. R. Akhmetshin *et al.*, Phys. Lett. **B578**, 285 (2004), hep-ex/0308008, Re-analysis of hadronic cross section measurements at CMD- 2.
- [20] CMD-2, R. R. Akhmetshin *et al.*, Phys. Lett. **B648**, 28 (2007), hep-ex/0610021, High-statistics measurement of the pion form factor in the rho-meson energy range with the CMD-2 detector.
- [21] M. N. Achasov *et al.*, J. Exp. Theor. Phys. **103**, 380 (2006), hep-ex/0605013, Update of the  $e^+e^- \rightarrow \pi^+\pi^-$  cross section measured by SND detector in the energy region  $400\text{-MeV} < \sqrt{s} < 1000\text{-MeV}$ .
- [22] Particle Data Group, C. Amsler *et al.*, Phys. Lett. **B667**, 1 (2008), Review of particle physics.
- [23] S. Ghozzi and F. Jegerlehner, Phys. Lett. **B583**, 222 (2004), hep-ph/0310181, Isospin violating effects in e+e- vs. tau measurements of the pion form factor  $|F_\pi|^2(s)$ .
- [24] M. Bando, T. Kugo, and K. Yamawaki, Nucl. Phys. **B259**, 493 (1985), On the Vector Mesons as Dynamical Gauge Bosons of Hidden Local Symmetries.

- [25] M. Benayoun and H. B. O’Connell, Phys. Rev. **D58**, 074006 (1998), hep-ph/9804391, SU(3) breaking and hidden local symmetry.
- [26] W. J. Marciano and A. Sirlin, Phys. Rev. Lett. **71**, 3629 (1993), Radiative corrections to pi(lepton 2) decays.
- [27] V. Cirigliano, G. Ecker, and H. Neufeld, (2001), hep-ph/0109286, Isospin violation and the magnetic moment of the muon.
- [28] V. Cirigliano, G. Ecker, and H. Neufeld, Phys. Lett. **B513**, 361 (2001), hep-ph/0104267, Isospin violation and the magnetic moment of the muon.
- [29] V. Cirigliano, G. Ecker, and H. Neufeld, JHEP **08**, 002 (2002), hep-ph/0207310, Radiative tau decay and the magnetic moment of the muon.
- [30] BABAR, B. Aubert, (2009), 0912.0242, Measurements of Charged Current Lepton Universality and  $|V_{us}|$  using Tau Lepton Decays to  $e^- \bar{\nu}_e \nu_\tau$ ,  $\mu^- \bar{\nu}_\mu \nu_\tau$ ,  $\pi^- \nu_\tau$  and  $K^- \nu_\tau$ .
- [31] OPAL, K. Ackerstaff *et al.*, Eur. Phys. J. **C7**, 571 (1999), hep-ex/9808019, Measurement of the strong coupling constant  $\alpha_s$  and the vector and axial-vector spectral functions in hadronic tau decays.
- [32] CLEO, M. Artuso *et al.*, Phys. Rev. Lett. **72**, 3762 (1994), hep-ph/9404310, A Measurement of the branching fraction Beta ( $\tau^{+-} \rightarrow h^{+-} \pi^0 \tau$ -neutrino).
- [33] J.Urheim, private communication .
- [34] H. Hayashii, private communication .
- [35] CMD2, R. R. Akhmetshin *et al.*, Phys. Lett. **B605**, 26 (2005), hep-ex/0409030, Study of the Processes  $e^+e^- \rightarrow \eta\gamma$ ,  $e^+e^- \rightarrow \pi^0\gamma \rightarrow 3\gamma$  in the c.m. Energy Range 600–1380 MeV at CMD-2.
- [36] M. N. Achasov *et al.*, Eur. Phys. J. **C12**, 25 (2000), Experimental study of the processes  $e^+e^- \rightarrow \phi \rightarrow \eta\gamma, \pi^0\gamma$  at VEPP-2M.
- [37] M. N. Achasov *et al.*, Phys. Lett. **B559**, 171 (2003), hep-ex/0302004, Experimental study of the  $e^+e^- \rightarrow \pi^0\gamma$  process in the energy region  $\sqrt{s} = 0.60 - 0.97$  GeV.
- [38] CMD2, R. R. Akhmetshin *et al.*, Phys. Lett. **B460**, 242 (1999), hep-ex/9907003, Study of the radiative decay  $\phi \rightarrow \eta\gamma$  with CMD-2 detector.
- [39] CMD-2, R. R. Akhmetshin *et al.*, Phys. Lett. **B509**, 217 (2001), hep-ex/0103043, Study of the Process  $e^+e^- \rightarrow \eta\gamma$  in c.m. Energy Range 600-1380 MeV at CMD-2.
- [40] M. N. Achasov *et al.*, Phys. Rev. **D76**, 077101 (2007), 0709.1007, Reanalysis of the  $e^+e^- \rightarrow \eta\gamma$  reaction cross section.
- [41] S. I. Dolinsky *et al.*, Phys. Rept. **202**, 99 (1991), Summary of experiments with the neutral detector at the  $e^+e^-$  storage ring VEPP-2M.

- [42] CMD, L. M. Barkov *et al.*, (1989), BudkerINP preprint 89-15, Novosibirsk.
- [43] R. R. Akhmetshin *et al.*, Phys. Lett. **B642**, 203 (2006), Study of  $\phi \rightarrow \pi^+\pi^-\pi^0$  with CMD-2 detector.
- [44] R. R. Akhmetshin *et al.*, Phys. Lett. **B364**, 199 (1995), Measurement of phi meson parameters with CMD-2 detector at VEPP-2M collider.
- [45] R. R. Akhmetshin *et al.*, Phys. Lett. **B434**, 426 (1998), Study of dynamics of  $\phi \rightarrow \pi^+\pi^-\pi^0$  decay with CMD-2 detector.
- [46] M. N. Achasov *et al.*, Phys. Rev. **D66**, 032001 (2002), hep-ex/0201040, Study of the process  $e^+e^- \rightarrow \pi^+\pi^-\pi^0$  in the energy region  $\sqrt{s}$  from 0.98 to 1.38 GeV.
- [47] M. N. Achasov *et al.*, Phys. Rev. **D68**, 052006 (2003), hep-ex/0305049, Study of the process  $e^+e^- \rightarrow \pi^+\pi^-\pi^0$  in the energy region  $\sqrt{s}$  below 0.98 GeV.
- [48] R. R. Akhmetshin *et al.*, JETP Lett. **84**, 413 (2006), hep-ex/0610016, Measurement of the  $e^+e^- \rightarrow \pi^+\pi^-$  cross section with the CMD-2 detector in the 370-MeV - 520-MeV cm energy range.
- [49] L. M. Barkov *et al.*, Nucl. Phys. **B256**, 365 (1985), Electromagnetic Pion Form-Factor in the Timelike Region.
- [50] S. Eidelman, private communication .
- [51] A. Quenzer *et al.*, Phys. Lett. **B76**, 512 (1978), Pion Form-Factor from 480-MeV to 1100-MeV.
- [52] J. Schwinger, Particles, Sources and Fields, Vol II , Addison–Wesley, Reading, MA, 1970–1973.
- [53] M. Drees and K.-i. Hikasa, Phys. Lett. **B252**, 127 (1990), Scalar top production in  $e^+e^-$  annihilation.
- [54] KLOE, G. Venanzoni *et al.*, (2009), 0906.4331, A precise new KLOE measurement of  $|F_\pi|^2$  with ISR events and determination of  $\pi\pi$  contribution to  $a_\mu$  for  $0.592 < M_{\pi\pi} < 0.975$  GeV.
- [55] Z. Zhang, private communication .
- [56] G. Colangelo, Nucl. Phys. Proc. Suppl. **B 131**, 185 (2004), Hadronic contributions to  $a_\mu$  below one GeV.
- [57] G. Colangelo, Nucl. Phys. Proc. Suppl. **B 162**, 256 (2006), Chiral Symmetry,  $\pi\pi$  scattering and  $a_\mu$ .
- [58] KLOE, Müller. *et al.*, KLOE Note **221** (2008), [www.inf.it/kloe/pub/knote/kn221.pdf](http://www.inf.it/kloe/pub/knote/kn221.pdf), Measurement of  $\sigma(e^+e^- \rightarrow \pi^+\pi^-\gamma(\gamma))$  and the dipion contribution to the muon anomaly with the KLOE detector.

- [59] BABAR, . B. Aubert, (2009), 0908.3589, Precise measurement of the  $e^+ e^-$  to  $\pi^+ \pi^- (\gamma)$  cross section with the Initial State Radiation method at BABAR.
- [60] M. Davier, A. Hoecker, B. Malaescu, C. Z. Yuan, and Z. Zhang, (2009), 0908.4300, Reevaluation of the hadronic contribution to the muon magnetic anomaly using new  $e^+ e^- \rightarrow \pi^+ \pi^-$  cross section data from BABAR.
- [61] M. Davier, Nucl. Phys. B Proc. Suppl. **189**, 222 (2009), Measurement of the  $e^+ e^- \rightarrow \pi^+ \pi^- (\gamma)$  Cross section with the ISR Method with BABAR.
- [62] M. Benayoun, L. Del Buono, P. David, and O. Leitner, (2009), 0912.1248, Can VMD improve the estimate of the muon  $g-2$  ?

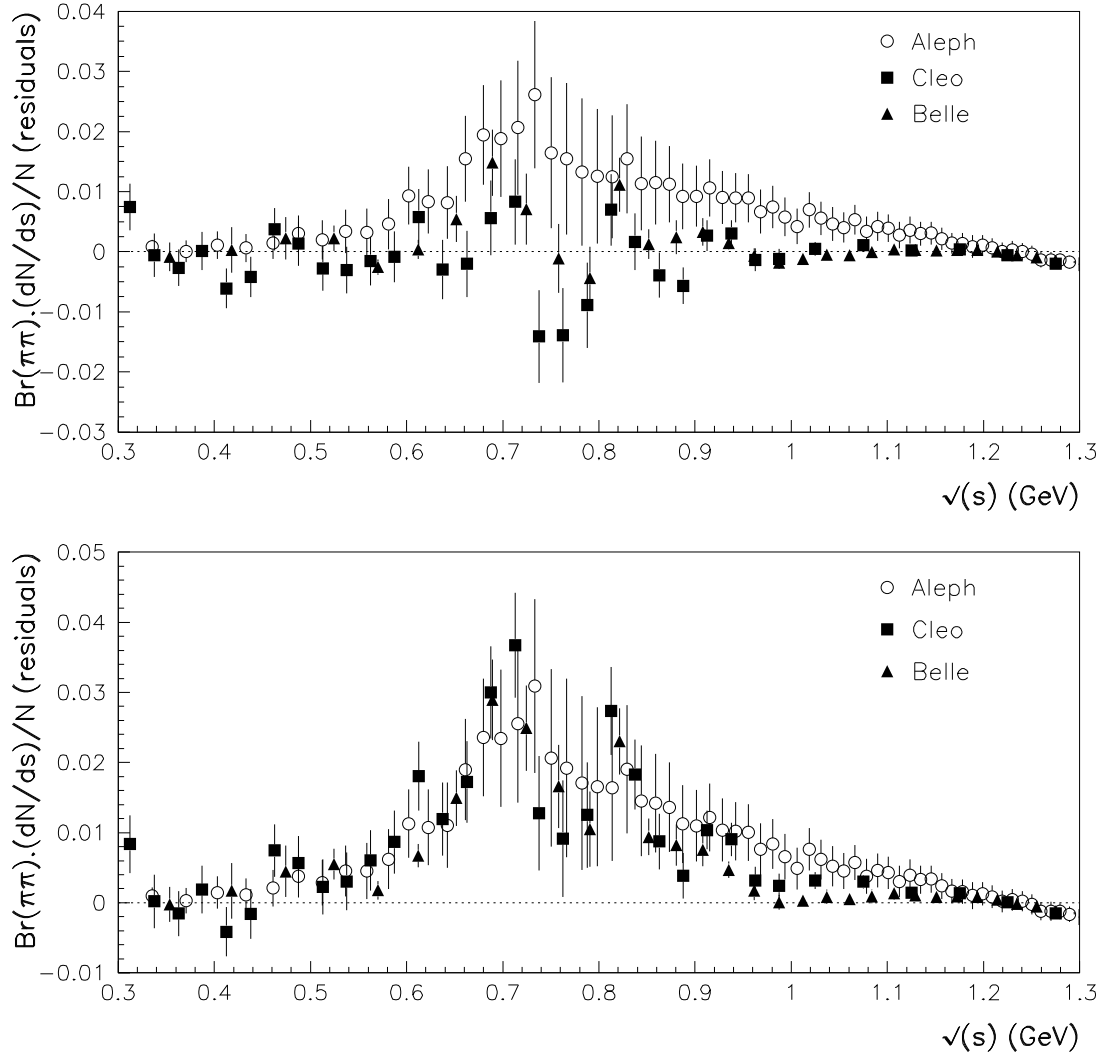


Figure 1: Residual distributions of ALEPH [15], BELLE [17] and CLEO [16] data sets in fits with mass and width differences between the charged and neutral  $\rho$  mesons. Upmost Figure includes fit rescaling factors constrained by the experimental uncertainty on  $\mathcal{B}_{\pi\pi}$ ; downmost Figure corresponds to assuming no rescaling. The fit region is bounded by  $1 \text{ GeV}/c$ .

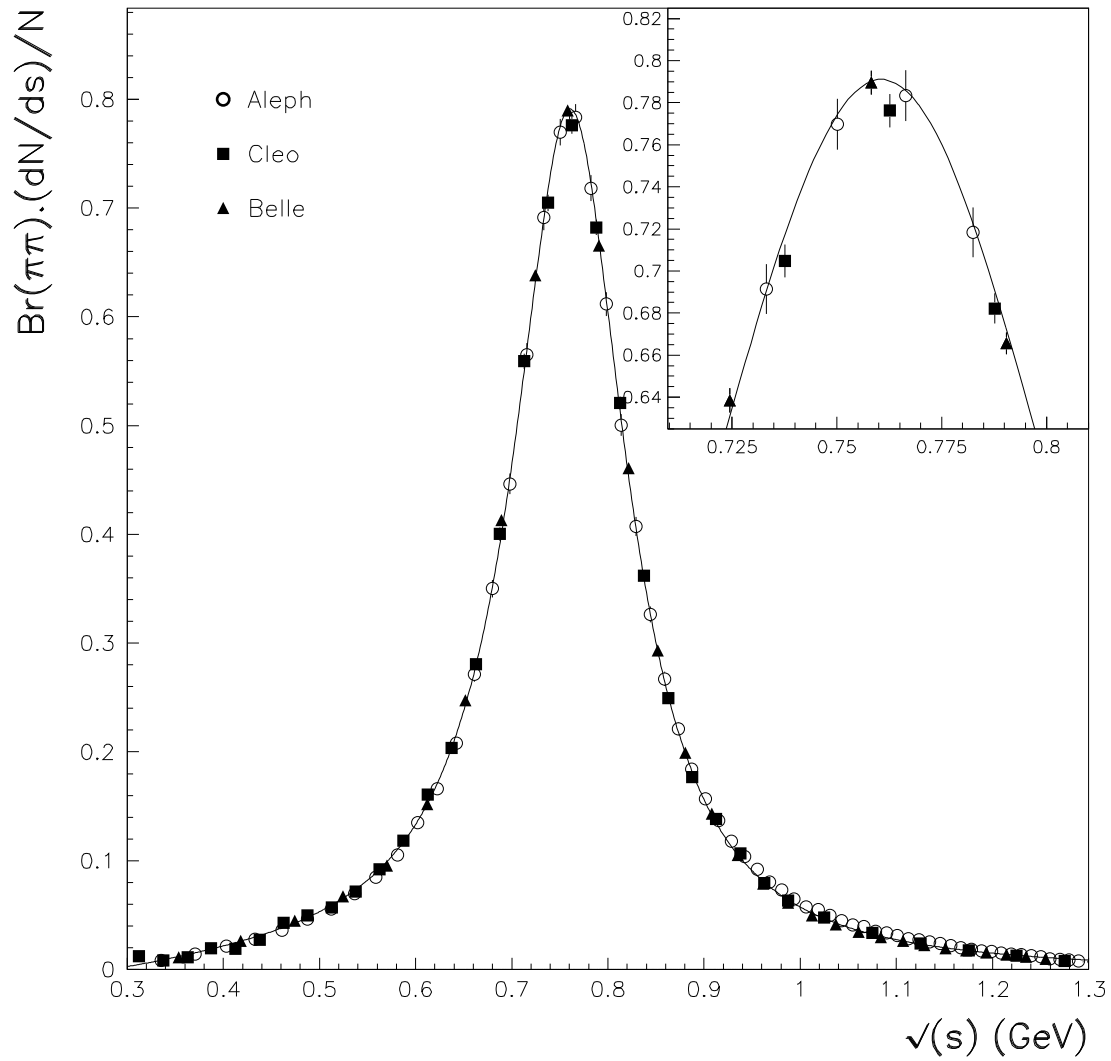


Figure 2: Fit to the  $\tau$  spectra from ALEPH [15], BELLE [17] and CLEO [16] data sets. The absolute normalization of the  $\tau$  spectra is completely free.

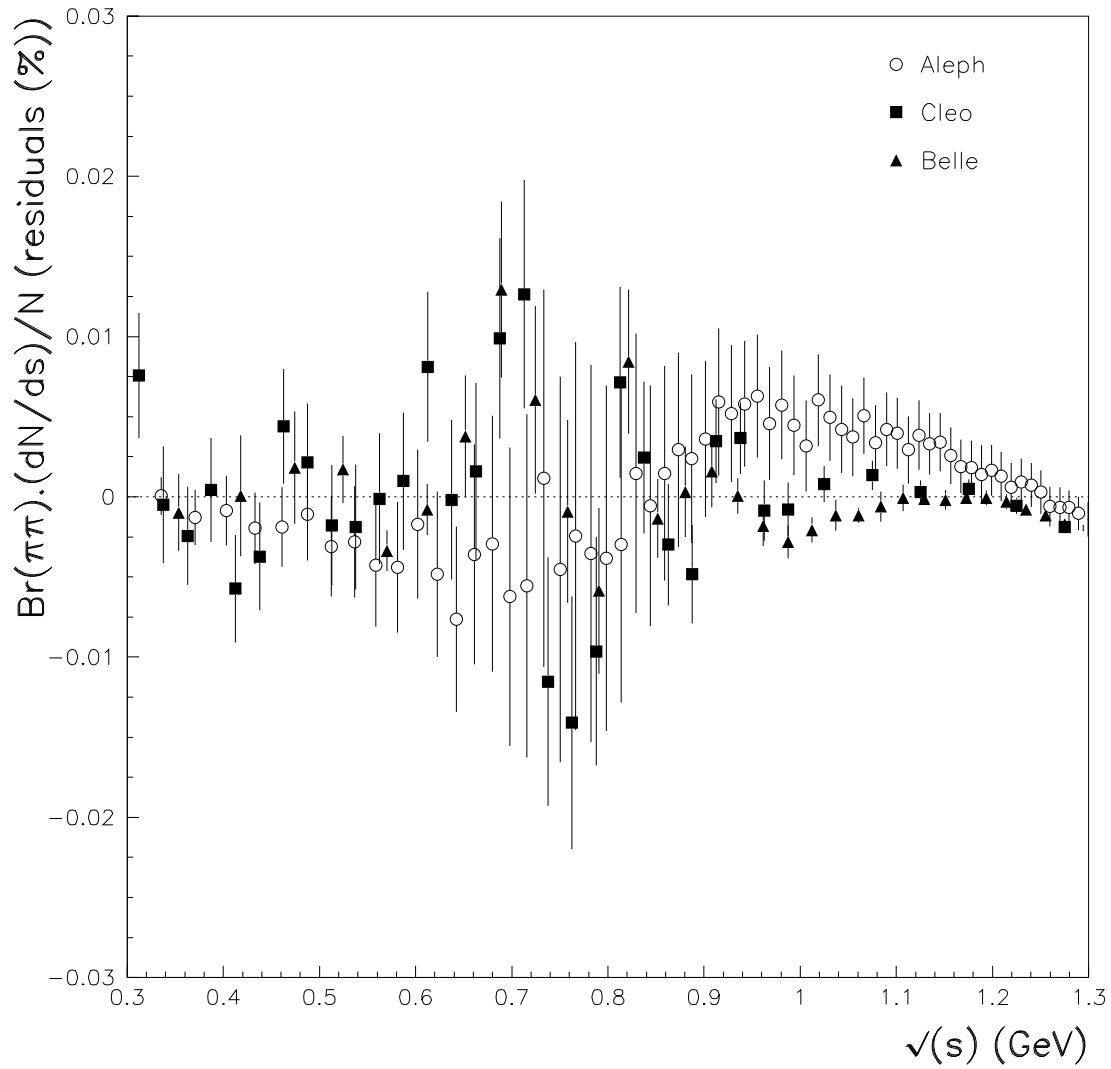


Figure 3: Residuals distribution in the fit to the  $\tau$  spectra from ALEPH [15], BELLE [17] and CLEO [16] data sets. The absolute normalization of the  $\tau$  spectra is completely free.

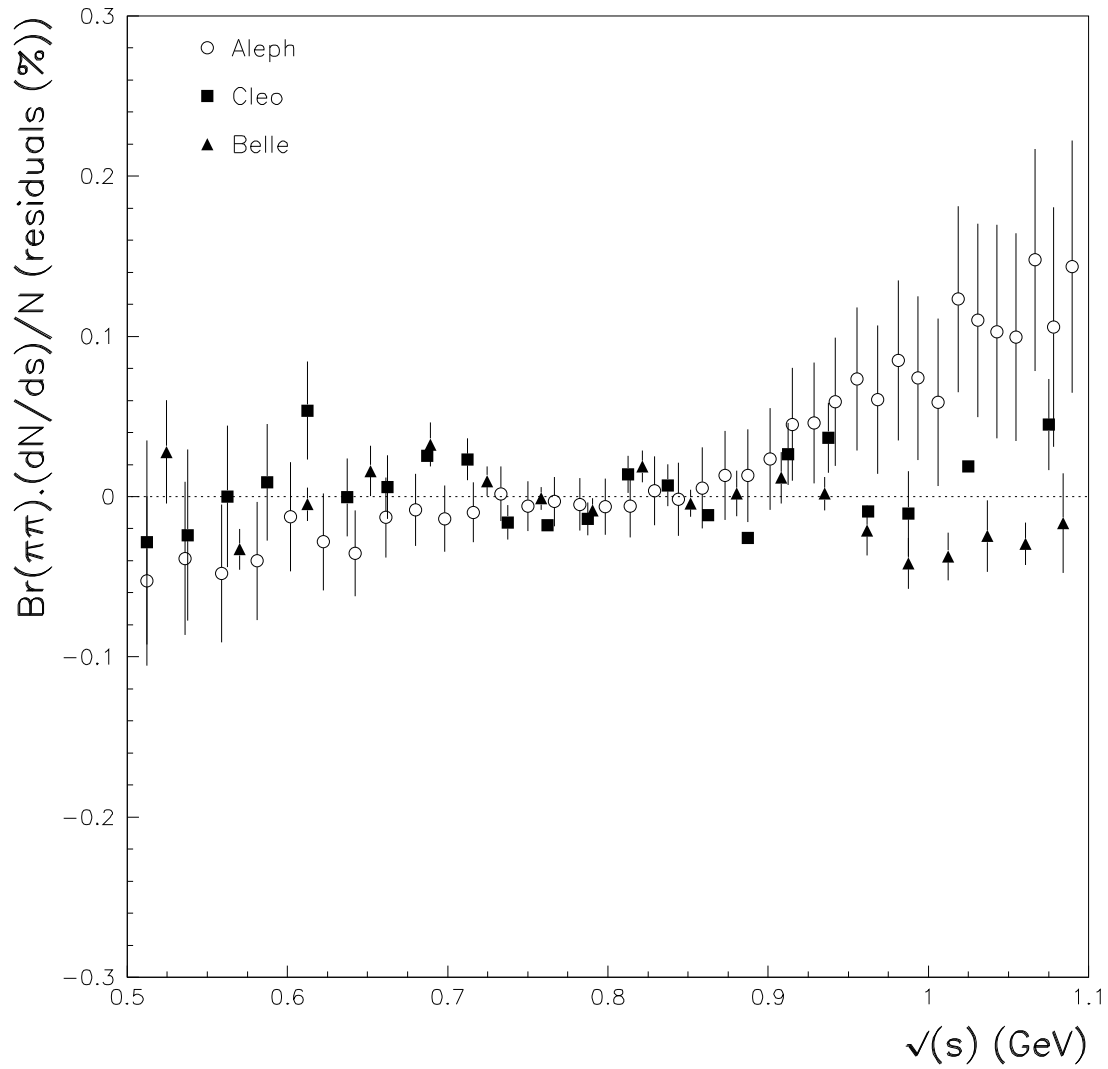


Figure 4: Residuals distribution in the fit to the  $\tau$  spectra from ALEPH [15], BELLE [17] and CLEO [16] data sets. The residuals are normalized too the fit function values. The absolute normalization of the  $\tau$  spectra was left completely free.



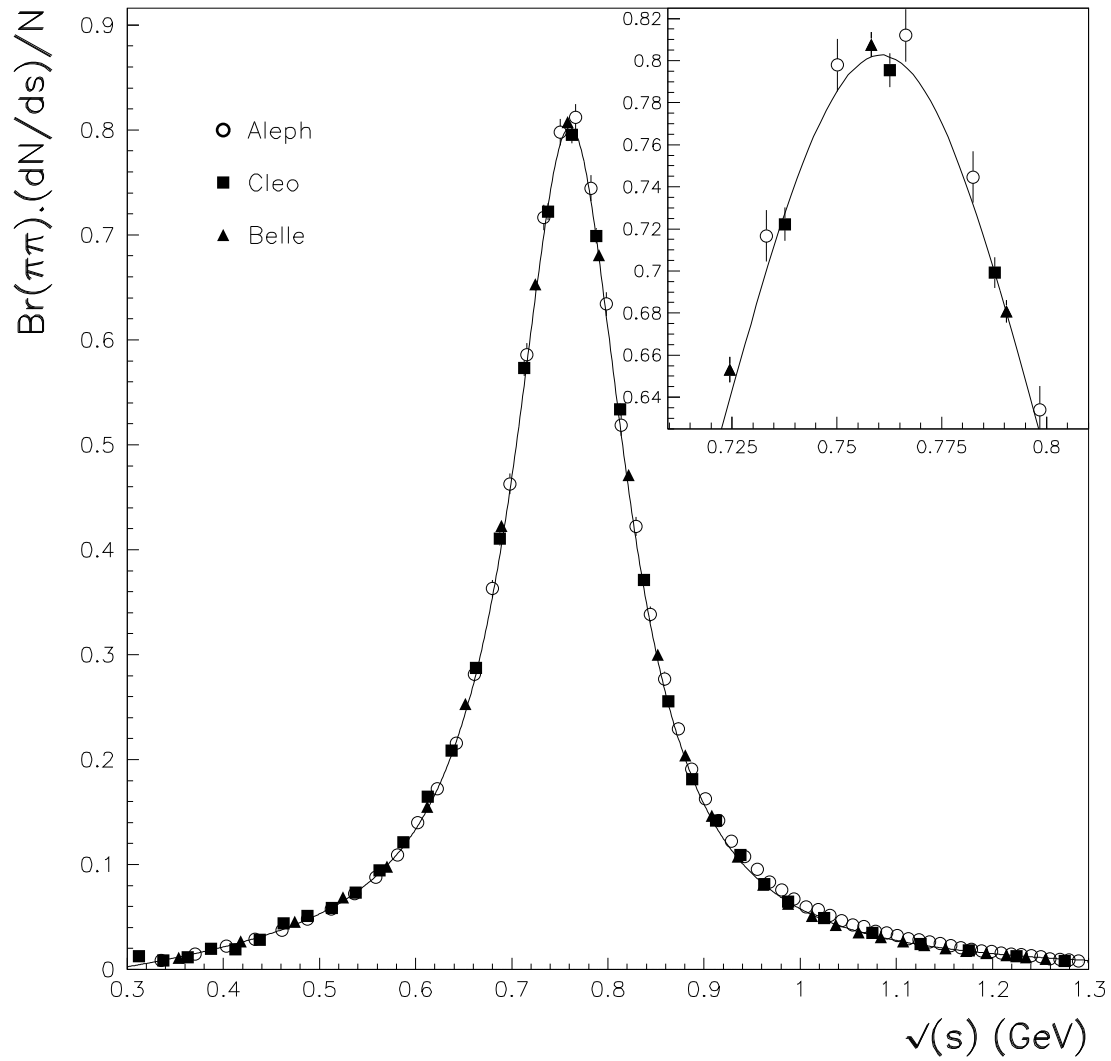


Figure 5: Fit to the  $\tau$  spectra from ALEPH [15], BELLE [17] and CLEO [16] data sets. The normalization is fit but constrained by the experimental uncertainties on  $B_{\pi\pi}$  (see text).

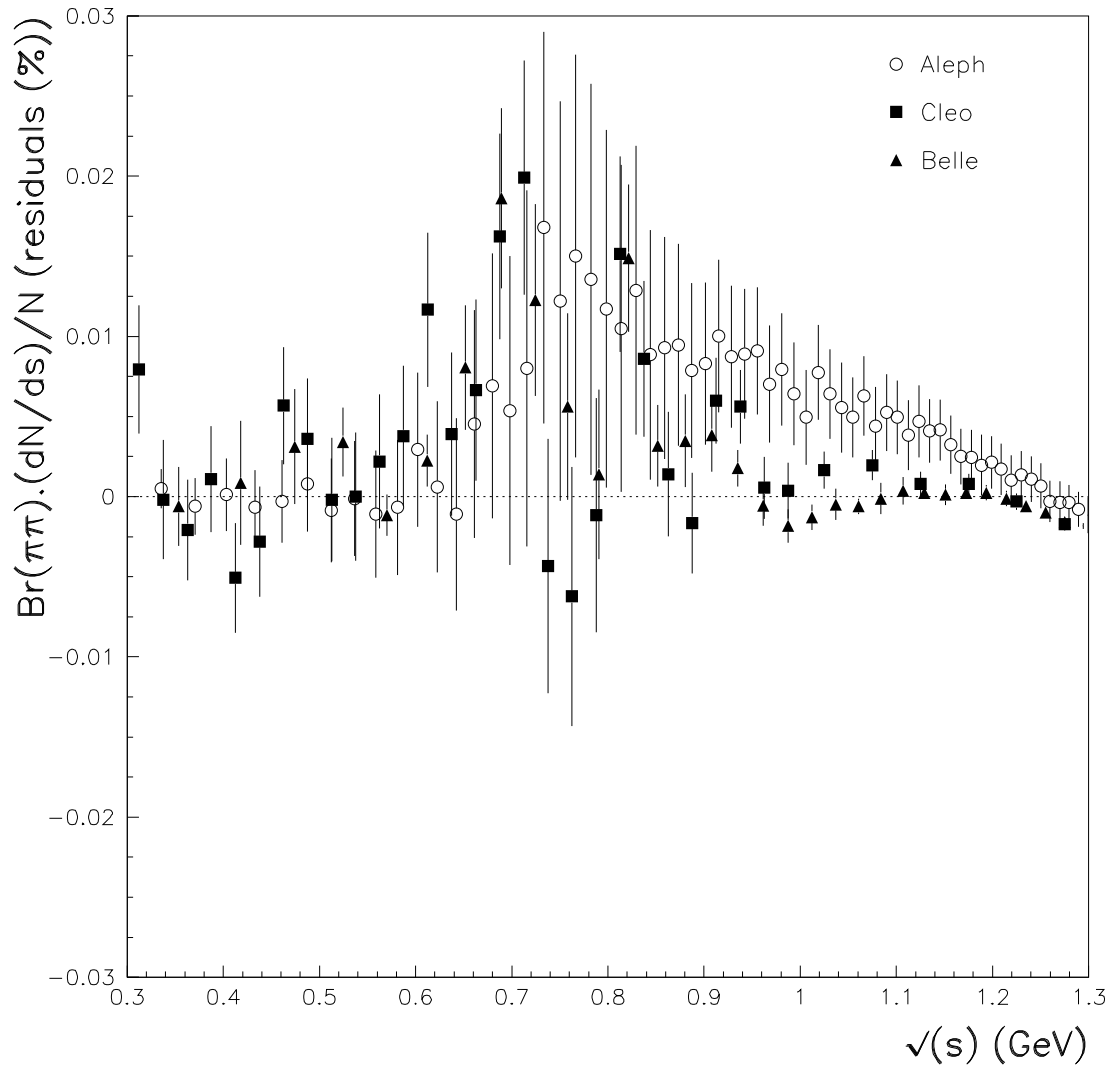


Figure 6: Residuals distribution in the fit to the  $\tau$  spectra from ALEPH [15], BELLE [17] and CLEO [16] data sets. The normalization is fit but constrained by the experimental uncertainties on  $B_{\pi\pi}$  (see text).

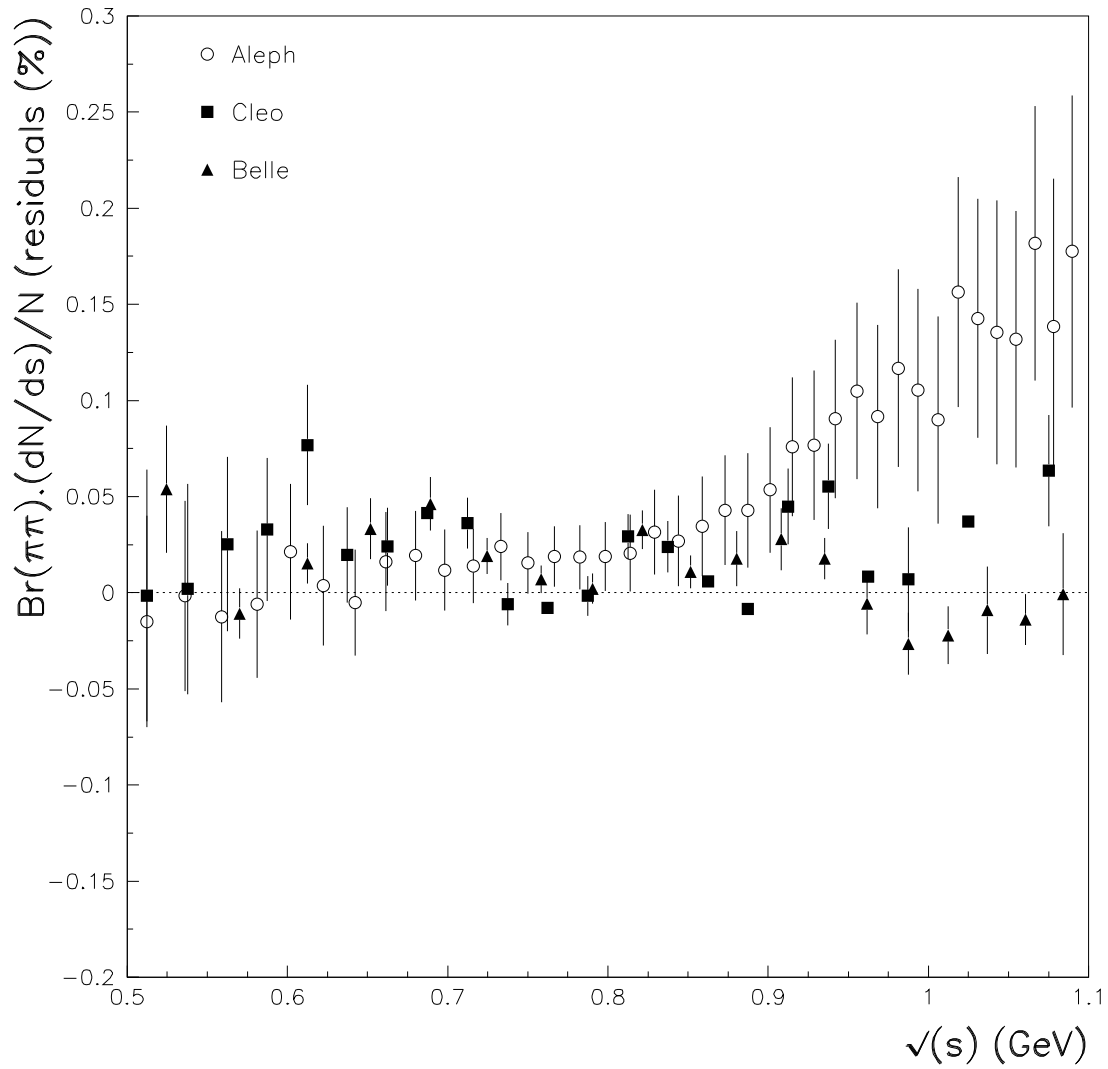


Figure 7: Residuals distribution in the fit to the  $\tau$  spectra from ALEPH [15], BELLE [17] and CLEO [16] data sets. The residuals are normalized too the fit function values. The absolute normalization of the  $\tau$  spectra was constrained by the uncertainty on  $B_{\pi\pi}$  (see text).

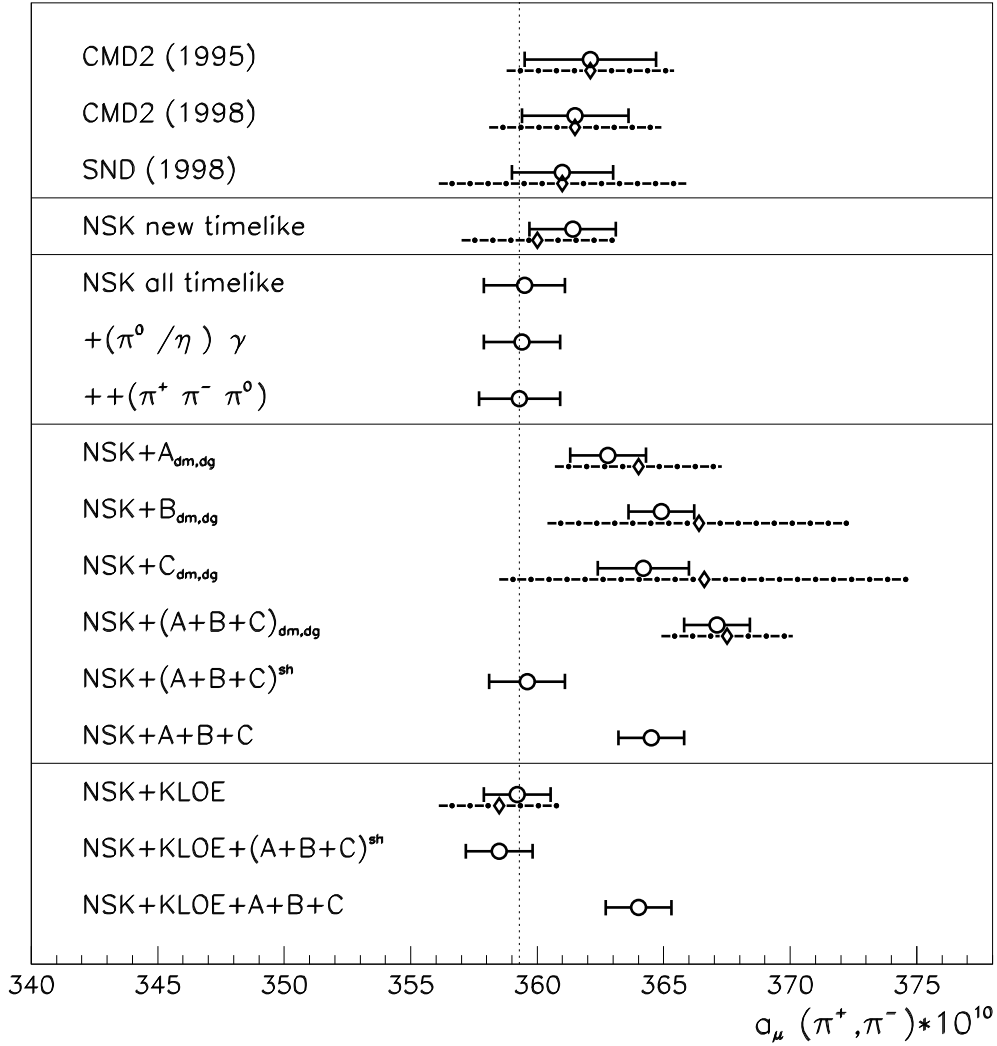


Figure 8: Values of  $a_\mu(\pi\pi) \times 10^{10}$  integrated between 0.630 and 0.958 GeV. Data configurations have been defined in Table 4 for the first seven lines, and in Tables 5 and 6 for the following lines. The various notations used for the  $\tau$  data samples have been defined in the text. The points with dashed–dotted uncertainties are experimental values provided by the experiments [19, 20, 21] or in [14].